

Stable Phase Field Approximations of Anisotropic Solidification

John W. Barrett[†] Harald Garcke[‡] Robert Nürnberg[†]

Abstract

We introduce unconditionally stable finite element approximations for a phase field model for solidification, which take highly anisotropic surface energy and kinetic effects into account. We hence approximate Stefan problems with anisotropic Gibbs–Thomson law with kinetic undercooling, and quasi-static variants thereof. The phase field model is given by

$$\begin{aligned} \vartheta w_t + \lambda \varrho(\varphi) \varphi_t &= \nabla \cdot (b(\varphi) \nabla w), \\ c_\Psi \frac{a}{\alpha} \varrho(\varphi) w &= \varepsilon \frac{\rho}{\alpha} \mu(\nabla \varphi) \varphi_t - \varepsilon \nabla \cdot A'(\nabla \varphi) + \varepsilon^{-1} \Psi'(\varphi) \end{aligned}$$

subject to initial and boundary conditions for the phase variable φ and the temperature approximation w . Here $\varepsilon > 0$ is the interfacial parameter, Ψ is a double well potential, $c_\Psi = \int_{-1}^1 \sqrt{2} \Psi(s) \, ds$, ϱ is a shape function and $A(\nabla \varphi) = \frac{1}{2} |\gamma(\nabla \varphi)|^2$, where γ is the anisotropic density function. Moreover, $\vartheta \geq 0$, $\lambda > 0$, $a > 0$, $\alpha > 0$ and $\rho \geq 0$ are physical parameters from the Stefan problem, while b and μ are coefficient functions which also relate to the sharp interface problem.

On introducing the novel fully practical finite element approximations for the anisotropic phase field model, we prove their stability and demonstrate their applicability with some numerical results.

Key words. phase field models, parabolic partial differential equations, Stefan problem, anisotropy, Allen–Cahn equation, viscous Cahn–Hilliard equation, crystal growth, finite element approximation

AMS subject classifications. 65M60, 65M12, 35K55, 74N20

1 Introduction

Phase field models are a successful approach for interface evolution in cases where interfacial energy is important, and many numerical approaches for the underlying equations

[†]Department of Mathematics, Imperial College London, London, SW7 2AZ, UK

[‡]Fakultät für Mathematik, Universität Regensburg, 93040 Regensburg, Germany

have been studied in the literature. However, in situations where anisotropy is incorporated only very few results related to the numerical analysis of approximations to the phase field system have appeared in the literature. The reason for this is that the underlying equations involve highly nonlinear parabolic partial differential equations. Since phase field models describe very unstable solidification phenomena, it seems to be very important to use stable approximation schemes which do not trigger additional instabilities resulting from discretization errors. In this context we would like to mention that there exist many computations on anisotropic solidification, with the help of phase field equations, showing pattern formation which is driven by the discretization rather than by the underlying partial differential equations. The goal of this paper is to introduce and analyze a new stable finite element approximation for the anisotropic phase field system. The approach is based on earlier work for the Allen–Cahn and the Cahn–Hilliard equations, see Barrett *et al.* (2012c), and on ideas on how to handle the anisotropy that have been used earlier for sharp interface models by the same authors, see Barrett *et al.* (2008a,b). To our knowledge, the introduced finite element approximation is the first unconditionally stable approximation of a phase field model for anisotropic solidification in the literature.

As the phase field model and its quasi-stationary variant, the viscous Cahn–Hilliard equation, converge to sharp interface models for solidification in the asymptotic limit as the interfacial thickness tends to zero we first introduce the sharp interface model. Let $\Gamma(t) \subset \mathbb{R}^d$, $d = 2, 3$, denote the interface between a solid and liquid phase, say, or a solid phase and a gas phase. Then the surface energy of $\Gamma(t)$ is defined as

$$\int_{\Gamma(t)} \gamma(\mathbf{n}) \, ds, \quad (1.1)$$

where \mathbf{n} denotes the unit normal of $\Gamma(t)$, and where the anisotropic density function $\gamma : \mathbb{R}^d \rightarrow \mathbb{R}_{\geq 0}$ with $\gamma \in C^2(\mathbb{R}^d \setminus \{0\}) \cap C(\mathbb{R}^d)$ is assumed to be absolutely homogeneous of degree one, i.e.

$$\gamma(\lambda p) = |\lambda| \gamma(p) \quad \forall p \in \mathbb{R}^d, \quad \forall \lambda \in \mathbb{R} \quad \Rightarrow \quad \gamma'(p) \cdot p = \gamma(p) \quad \forall p \in \mathbb{R}^d \setminus \{0\}, \quad (1.2)$$

with γ' denoting the gradient of γ .

Relevant for our considerations is the first variation, $-\kappa_\gamma$, of (1.1), which can be computed as

$$\kappa_\gamma := -\nabla_s \cdot \gamma'(\mathbf{n});$$

where ∇_s is the tangential divergence of Γ , see e.g. Cahn and Hoffman (1974); Barrett *et al.* (2008b, 2010b). Note that κ_γ reduces to the sum of the principal curvatures of Γ in the isotropic case, i.e. when γ satisfies

$$\gamma(p) = |p| \quad \forall p \in \mathbb{R}^d. \quad (1.3)$$

Then the full Stefan problem that we want to consider in this paper is given as follows, where $\Omega \subset \mathbb{R}^d$ is a given fixed domain with boundary $\partial\Omega$ and outer normal ν .

Find $u : \Omega \times [0, T] \rightarrow \mathbb{R}$ and the interface $(\Gamma(t))_{t \in [0, T]}$ such that for all $t \in (0, T]$ the following conditions hold:

$$\vartheta u_t - \mathcal{K}_- \Delta u = 0 \quad \text{in } \Omega_-(t), \quad \vartheta u_t - \mathcal{K}_+ \Delta u = 0 \quad \text{in } \Omega_+(t), \quad (1.4a)$$

$$\left[\mathcal{K} \frac{\partial u}{\partial \mathbf{n}} \right]_{\Gamma(t)} = -\lambda \mathcal{V} \quad \text{on } \Gamma(t), \quad (1.4b)$$

$$\frac{\rho \mathcal{V}}{\beta(\mathbf{n})} = \alpha \kappa_\gamma - a u \quad \text{on } \Gamma(t), \quad (1.4c)$$

$$\frac{\partial u}{\partial \nu} = 0 \quad \text{on } \partial_N \Omega, \quad u = u_D \quad \text{on } \partial_D \Omega, \quad (1.4d)$$

$$\Gamma(0) = \Gamma_0, \quad \vartheta u(\cdot, 0) = \vartheta u_0 \quad \text{in } \Omega. \quad (1.4e)$$

In the above u denotes the deviation from the melting temperature T_M , i.e. T_M is the melting temperature for a planar interface. In addition, $\Omega_-(t)$ is the solid region, with boundary $\Gamma(t) = \partial\Omega_-(t)$, so that the liquid region is given by $\Omega_+(t) := \Omega \setminus \overline{\Omega_-(t)}$. Here we assume that the solid region $\overline{\Omega_-(t)}$ has no intersection with the external boundary $\partial\Omega$, but more general situations can also be considered, as will be outlined in Section 3 below. Moreover, here and throughout this paper, for a quantity v defined on Ω , we use the shorthand notations $v_- := v|_{\Omega_-}$ and $v_+ := v|_{\Omega_+}$. The parameters $\vartheta \geq 0$, $\lambda > 0$, $\rho \geq 0$, $\alpha > 0$, $a > 0$ are assumed to be constant, while $\mathcal{K}_\pm > 0$ are assumed to be constant in each phase. The mobility coefficient $\beta : \mathbb{R}^d \rightarrow \mathbb{R}_{\geq 0}$ is assumed to satisfy $\beta(p) > 0$ for all $p \neq 0$ and to be positively homogeneous of degree one. In addition $[\mathcal{K} \frac{\partial u}{\partial \mathbf{n}}]_{\Gamma(t)}(z) := (\mathcal{K}_+ \frac{\partial u_+}{\partial \mathbf{n}} - \mathcal{K}_- \frac{\partial u_-}{\partial \mathbf{n}})(z)$ for all $z \in \Gamma(t)$, and \mathcal{V} is the velocity of $\Gamma(t)$ in the direction of its normal \mathbf{n} , which from now on we assume is pointing into $\Omega_+(t)$. Finally, $\partial\Omega = \partial_N \Omega \cup \partial_D \Omega$ with $\partial_N \Omega \cap \partial_D \Omega = \emptyset$, $u_D : \partial_D \Omega \rightarrow \mathbb{R}$ is the applied supercooling at the boundary, and $\Gamma_0 \subset \overline{\Omega}$ and $u_0 : \Omega \rightarrow \mathbb{R}$ are given initial data.

The model (1.4a–e) can be derived for example within the theory of rational thermodynamics and we refer to Gurtin (1988) for details. We remark that a derivation from thermodynamics would lead to the identity $a = \frac{\lambda}{T_M}$. We note that (1.4b) is the well-known Stefan condition, while (1.4c) is the Gibbs–Thomson condition, with kinetic undercooling if $\rho > 0$. The case $\vartheta > 0$, $\rho > 0$, $\alpha > 0$ leads to the Stefan problem with the Gibbs–Thomson law and kinetic undercooling. In some models in the literature, see e.g. Luckhaus (1990), the kinetic undercooling is set to zero, i.e. $\rho = 0$. Setting $\vartheta = \rho = 0$ but keeping $\alpha > 0$ leads to the Mullins–Sekerka problem with the Gibbs–Thomson law, see Mullins and Sekerka (1963).

For later reference, we introduce the function spaces

$$S_0 := \{\eta \in H^1(\Omega) : \eta = 0 \text{ on } \partial_D \Omega\} \quad \text{and} \quad S_D := \{\eta \in H^1(\Omega) : \eta = u_D \text{ on } \partial_D \Omega\},$$

where we assume for simplicity of the presentation from now on that

$$\begin{aligned} &\text{either (i) } \partial\Omega = \partial_D \Omega, \quad \text{(ii) } \partial\Omega = \partial_N \Omega, \\ &\text{or (iii) } \Omega = (-H, H)^d, \quad \partial_D \Omega = [-H, H]^{d-1} \times \{H\}, \quad H > 0; \end{aligned} \quad (1.5)$$

and, in the cases (1.5)(i) and (iii), that $u_D \in H^{\frac{1}{2}}(\partial_D \Omega)$. For notational convenience, we define $u_D := 0$ in the case (1.5)(ii).

We recall from Barrett *et al.* (2010b) that, on assuming that u_D is constant, for a solution u and Γ to (1.4a–e) it can be shown that the following formal energy equality holds

$$\begin{aligned} \frac{d}{dt} \left(\frac{\vartheta}{2} |u - u_D|_0^2 + \frac{\lambda \alpha}{a} \int_{\Gamma(t)} \gamma(\mathbf{n}) \, ds - \lambda u_D |\Omega_+(t)| \right) + (\mathcal{K} \nabla u, \nabla u) \\ + \frac{\lambda \rho}{a} \int_{\Gamma(t)} \frac{\mathcal{V}^2}{\beta(\mathbf{n})} \, ds = 0, \quad (1.6) \end{aligned}$$

where (\cdot, \cdot) denotes the L^2 -inner product over Ω , with the corresponding norm given by $|\cdot|_0$, and where $|\Omega_+(t)| := \int_{\Omega_+(t)} 1 \, dx$.

In Section 2 we will precisely state a phase field model which approximates the free boundary problem (1.4a–e). We only mention here that the phase field method is based on the idea of a diffuse interface, which hence has a positive thickness. Let us briefly discuss some relevant literature. For solidification the phase field method was originally proposed by Langer (1986) as a model for solidification of a pure substance. It was Kobayashi (1993) who first was able to simulate complicated dendritic patterns which resemble those appearing during solidification. Since then an enormous effort has gone into numerically studying phase field models. We refer only to Elliott and Gardiner (1996); Karma and Rappel (1996, 1998) and to the reviews Boettinger *et al.* (2002); Chen (2002); McFadden (2002); Singer-Loginova and Singer (2008).

A phase field model, and its numerical approximation, for the sharp interface problem (1.4a–e) with $\vartheta = \rho = 0$ and $\mathcal{K}_+ = \mathcal{K}_-$ has been considered in the recent paper Barrett *et al.* (2012c). In particular, the authors were able to present unconditionally stable finite element approximations, where the treatment of the anisotropy does not lead to new nonlinearities compared to the isotropic situation. It is one of the aims of the present article to extend the discretizations in Barrett *et al.* (2012c) to the more general problem (1.4a–e), i.e. in particular to the case $\vartheta > 0$, and $\rho > 0$, and to a wider class of anisotropies than considered in Barrett *et al.* (2012c). The new anisotropies considered in the present article will lead to more nonlinear schemes, however.

The remainder of the paper is organized as follows. In Section 2 we state the two phase field models for the approximation of the sharp interface problem (1.4a–e) that we want to consider in this paper. In Section 3 we introduce our finite element approximations for these problems, and we prove stability results for these approximations. Solution methods for the discrete equations are shortly reviewed in Section 4. In addition, we present several numerical experiments in Section 5.

2 Phase field models and anisotropies

Phase field models are a computational tool to compute approximations for sharp interface evolutions such as (1.4a–e), without having to capture the sharp interface $\Gamma(t)$ directly. On introducing a phase field $\varphi : \Omega \times (0, T) \rightarrow \mathbb{R}$, where the sets $\Omega_{\pm}^{\varepsilon}(t) := \{x \in \Omega : \pm\varphi(x, t) > 0\}$ are approximations to $\Omega_{\pm}(t)$, a system of partial differential equations for φ can be derived so that the zero level sets of φ formally approximate the interface $\Gamma(t)$, satisfying e.g. (1.4a–e), in a well defined limit. For more details on phase field methods and other approaches to the approximation of the evolution of interfaces we refer to the review article Deckelnick *et al.* (2005) and the references therein.

On introducing the small interfacial parameter $\varepsilon > 0$, it can be shown that

$$\frac{1}{c_{\Psi}} \mathcal{E}_{\gamma}(\varphi) \approx \int_{\Gamma} \gamma(\mathbf{n}) \, ds,$$

for ε sufficiently small, where

$$\mathcal{E}_{\gamma}(\varphi) := \int_{\Omega} \frac{\varepsilon}{2} |\gamma(\nabla \varphi)|^2 + \varepsilon^{-1} \Psi(\varphi) \, dx \quad \text{with} \quad c_{\Psi} := \int_{-1}^1 \sqrt{2\Psi(s)} \, ds. \quad (2.1)$$

Here $\Psi : \mathbb{R} \rightarrow [0, \infty]$ is a double well potential, which for simplicity we assume to be symmetric and to have its global minima at ± 1 . The canonical example is

$$\Psi(s) := \frac{1}{4} (s^2 - 1)^2 \quad \Rightarrow \quad \Psi'(s) = s^3 - s \quad \text{and} \quad c_{\Psi} = \frac{1}{3} 2^{\frac{3}{2}}. \quad (2.2)$$

Another possibility is to choose

$$\Psi(s) := \begin{cases} \frac{1}{2} (1 - s^2) & |s| \leq 1, \\ \infty & |s| > 1, \end{cases} \quad \Rightarrow \quad c_{\Psi} = \frac{\pi}{2}; \quad (2.3)$$

see e.g. Blowey and Elliott (1992); Elliott and Gardiner (1996); Elliott (1997). Clearly the obstacle potential (2.3), which forces φ to stay within the interval $[-1, 1]$, is not differentiable at ± 1 . Hence, whenever we write $\Psi'(s)$ in the case (2.3) in this paper, we mean that the expression holds only for $|s| < 1$, and that in general a variational inequality needs to be employed. While it can be shown that the asymptotic interface thickness in phase field models with (2.1) for the isotropic surface energy (1.3) is proportional to ε , for anisotropic energy densities the asymptotic interface thickness is no longer uniform, but now also depends on γ and on $\nabla \varphi$, see e.g. Bellettini and Paolini (1996); Elliott and Schätzle (1996); Wheeler and McFadden (1996).

We remark that other, non-classical, phase field models are based on the energy

$$\int_{\Omega} |\nabla \varphi|^{-1} \gamma(\nabla \varphi) \left(\frac{\varepsilon}{2} |\nabla \varphi|^2 + \varepsilon^{-1} \Psi(\varphi) \right) \, dx \quad (2.4)$$

for e.g. the smooth double-well potential (2.2), see Torabi *et al.* (2009). The energy (2.4) has the advantage that the asymptotic interface thickness is now only determined by ε

(independently of γ and the orientation of the interface), whereas the disadvantage is that the resultant partial differential equations become more nonlinear and are singular at $\nabla \varphi = 0$. We note that higher order regularizations of the energies (2.1) and (2.4) in the case of a non-convex anisotropy density function γ , which lead to sixth order Cahn–Hilliard type equations, have been considered in e.g. Li *et al.* (2009).

We are not aware of any numerical analysis for discretizations of anisotropic phase field models for (1.4a–e) involving either (2.1) or (2.4).

We now state the two phase field models that we are going to consider in this paper. To this end, for $p \in \mathbb{R}^d$, let

$$A(p) = \frac{1}{2} |\gamma(p)|^2 \quad \Rightarrow \quad A'(p) = \begin{cases} \gamma(p) \gamma'(p) & p \neq 0, \\ 0 & p = 0, \end{cases} \quad (2.5)$$

and define

$$\mu(p) = \begin{cases} \frac{\gamma(p)}{\beta(p)} & p \neq 0, \\ \bar{\mu} & p = 0, \end{cases} \quad (2.6)$$

where $\bar{\mu} \in \mathbb{R}$ is a constant satisfying $\min_{p \neq 0} \frac{\gamma(p)}{\beta(p)} \leq \bar{\mu} \leq \max_{p \neq 0} \frac{\gamma(p)}{\beta(p)}$.

2.1 Viscous Cahn–Hilliard equation

A phase field model for (1.4a–e) with $\vartheta = \rho = 0$ has been recently studied by the authors in Barrett *et al.* (2012c). The case $\vartheta = 0$ and $\rho \geq 0$ gives rise to the following viscous Cahn–Hilliard equation for the anisotropic Ginzburg–Landau energy (2.1), where w is a phase field approximation to the (rescaled) temperature u :

$$\frac{1}{2} \lambda \varphi_t = \nabla \cdot (b(\varphi) \nabla w) \quad \text{in } \Omega_T := \Omega \times (0, T), \quad (2.7a)$$

$$\frac{1}{2} c_\Psi \frac{a}{\alpha} w = \varepsilon \frac{\rho}{\alpha} \mu(\nabla \varphi) \varphi_t - \varepsilon \nabla \cdot A'(\nabla \varphi) + \varepsilon^{-1} \Psi'(\varphi) \quad \text{in } \Omega_T, \quad (2.7b)$$

$$\frac{\partial \varphi}{\partial \nu} = 0, \quad \text{on } \partial \Omega \times (0, T), \quad (2.7c)$$

$$w = u_D \quad \text{on } \partial_D \Omega \times (0, T), \quad (2.7d)$$

$$b(\varphi) \frac{\partial w}{\partial \nu} = 0, \quad \text{on } \partial_N \Omega \times (0, T), \quad (2.7e)$$

$$\varphi(\cdot, 0) = \varphi_0 \quad \text{in } \Omega, \quad (2.7f)$$

where

$$b(s) = \frac{1}{2} (1 + s) \mathcal{K}_+ + \frac{1}{2} (1 - s) \mathcal{K}_-. \quad (2.8)$$

With the help of formal asymptotics, see e.g. McFadden *et al.* (1993); Wheeler and McFadden (1996); Bellettini and Paolini (1996), it can be shown that the sharp interface limit of (2.7a–f), i.e. the limit as $\varepsilon \rightarrow 0$, is given by the quasi-static Stefan problem (or

Mullins–Sekerka problem) (1.4a–e) with $\vartheta = 0$, and with u denoting the sharp interface limit of w .

We remark that the phase field analogue of the sharp interface energy identity (1.6) in the case $\vartheta = 0$ is given by the formal energy bound

$$\frac{d}{dt} \left(\frac{\lambda \alpha}{a} \frac{1}{c_\Psi} \mathcal{E}_\gamma(\varphi) - \frac{1}{2} \lambda u_D \int_\Omega \varphi \, dx \right) + (b(\varphi) \nabla w, \nabla w) + \varepsilon \frac{\lambda \rho}{a} \frac{1}{c_\Psi} (\mu(\nabla \varphi), (\varphi_t)^2) \leq 0 \quad (2.9)$$

for the phase field model (2.7a–f) with the potential (2.3). For smooth potentials such as (2.2) the energy law (2.9) holds with equality.

2.2 Heat equation coupled to Allen–Cahn

The second phase field model is based on the work in Elliott and Gardiner (1996), see also Kobayashi (1993); Karma and Rappel (1996) for other related approaches, and allows the sharp interface limit (1.4a–e) with $\vartheta \geq 0$. It consists of a heat equation for the phase field temperature approximation w coupled to an Allen–Cahn phase field equation for φ . In particular, we have the modified heat equation

$$\vartheta w_t + \lambda \varrho(\varphi) \varphi_t = \nabla \cdot (b(\varphi) \nabla w) \quad \text{in } \Omega_T, \quad (2.10a)$$

$$w = u_D \quad \text{on } \partial_D \Omega \times (0, T), \quad (2.10b)$$

$$b(\varphi) \frac{\partial w}{\partial \nu} = 0 \quad \text{on } \partial_N \Omega \times (0, T), \quad (2.10c)$$

$$\vartheta w(\cdot, 0) = \vartheta w_0 \quad \text{in } \Omega, \quad (2.10d)$$

where b is defined in (2.8), and where the function $\varrho \in C^1(\mathbb{R})$ is such that

$$\varrho(s) \geq 0 \quad \forall s \in [-1, 1], \quad \int_{-1}^1 \varrho(y) \, dy = 1 \quad \text{and} \quad P(s) := \int_{-1}^s \varrho(y) \, dy.$$

We note that P , which is a monotonically increasing function over the interval $[-1, 1]$ with $P(-1) = 0$ and $P(1) = 1$, is often called the interpolation function. In this paper, we follow the convention from Elliott and Gardiner (1996), where $\varrho = P'$ is called the shape function. More details on interpolation functions P , respectively shape functions ϱ , can be found in e.g. Wang *et al.* (1993); Garcke and Stinner (2006); Eck *et al.* (2006); Caginalp *et al.* (2008). In particular, if one also assumes symmetry, i.e.

$$\varrho(s) = \varrho(-s) \quad \forall s \in [-1, 1],$$

then a faster convergence of the phase field model to the sharp interface limit, as $\varepsilon \rightarrow 0$, can be shown on prescribing suitable first order corrections in ε for the remaining phase field parameters; see Karma and Rappel (1996, 1998); Eck *et al.* (2006); Garcke and Stinner (2006) for details. Possible choices of ϱ that will be considered in this paper are

$$(i) \quad \varrho(s) = \frac{1}{2}, \quad (ii) \quad \varrho(s) = \frac{1}{2} (1 - s), \quad (iii) \quad \varrho(s) = \frac{15}{16} (s^2 - 1)^2. \quad (2.11)$$

The heat equation (2.10a–d) is coupled to the following modified Allen–Cahn equation:

$$c_\Psi \frac{a}{\alpha} \varrho(\varphi) w = \varepsilon \frac{\rho}{\alpha} \mu(\nabla \varphi) \varphi_t - \varepsilon \nabla \cdot A'(\nabla \varphi) + \varepsilon^{-1} \Psi'(\varphi) \quad \text{in } \Omega_T, \quad (2.12a)$$

$$\frac{\partial \varphi}{\partial \nu} = 0 \quad \text{on } \partial\Omega \times (0, T), \quad (2.12b)$$

$$\varphi(\cdot, 0) = \varphi_0 \quad \text{in } \Omega. \quad (2.12c)$$

We remark that the phase field analogue of the sharp interface energy identity (1.6) is given by the formal energy bound

$$\begin{aligned} \frac{d}{dt} \left(\frac{\vartheta}{2} |w - u_D|^2 + \frac{\lambda \alpha}{a} \frac{1}{c_\Psi} \mathcal{E}_\gamma(\varphi) - \lambda u_D \int_\Omega P(\varphi) dx \right) + (b(\varphi) \nabla w, \nabla w) \\ + \varepsilon \frac{\lambda \rho}{a} \frac{1}{c_\Psi} (\mu(\nabla \varphi), (\varphi_t)^2) \leq 0 \end{aligned} \quad (2.13)$$

for the phase field model (2.10a–d), (2.12a–c) with the potential (2.3). For smooth potentials such as (2.2) the energy law (2.13) holds with equality. We remark that the energy decay in (2.13) for the phase field model (2.10a–d), (2.12a–c) means that the model can be said to be thermodynamically consistent. For more details on thermodynamically consistent phase field models we refer to e.g. Penrose and Fife (1990); Wang *et al.* (1993).

REMARK. 2.1. *We remark that in the special case $\vartheta = 0$, and if we choose (2.11)(i), then clearly (2.10a–d), (2.12a–c) collapses to the system (2.7a–f). Similarly, the energy law (2.13) in this case collapses to (2.9). Hence from now on in this paper, we will only consider the more general model (2.10a–d), (2.12a–c). Finally we note that the phase field model (2.7a–f) in the case $\rho = 0$ was recently considered in Barrett et al. (2012c).*

We observe that for ε small, on recalling that the thickness of the interfacial region goes to zero as $\varepsilon \rightarrow 0$, it holds that

$$\int_\Omega P(\varphi) dx \approx P(1) |\Omega_+^\varepsilon(t)| + P(-1) |\Omega_-^\varepsilon(t)| = |\Omega_+^\varepsilon(t)|, \quad (2.14)$$

which is a consequence of the fact that $P(\varphi)$ approximates the characteristic function of the liquid phase $\Omega_+(t)$. It is clear from (2.13) and (2.14) that for negative values of u_D , φ is encouraged to take on negative values, so that the approximate liquid region $\Omega_+^\varepsilon(t)$ shrinks, whereas positive values of u_D encourage φ to take on positive values, so that the liquid region grows. Of course, this is simply the phase field analogue of the sharp interface behaviour induced by (1.6). A side effect of the interpolation function P in (2.13), however, is that the function

$$G(s) = \alpha (a c_\Psi \varepsilon)^{-1} \Psi(s) - u_D P(s) \quad (2.15)$$

need no longer have local minima at $s = \pm 1$. This can result, for example, in undesired, artificial boundary layers for strong supercoolings, i.e. when $-u_D$ is large; see also Remarks 3.3 and 3.9 below. For smooth potentials Ψ , sufficient conditions for $s = \pm 1$ to

be local minimum points of $G(s)$ are $\varrho(\pm 1) = \varrho'(\pm 1) = 0$, which is evidently satisfied by (2.11)(iii). In fact, in applications phase field models for solidification almost exclusively use the quartic potential (2.2) together with this shape function; see e.g. Boettinger *et al.* (2002); Chen (2002); McFadden (2002).

For the obstacle potential (2.3) the situation is similar, although there is more flexibility in the possible choices of ϱ . In particular, here a sufficient condition for $G(s)$ to have local minima at $s = \pm 1$ is given by

$$\alpha (a c_\Psi \varepsilon)^{-1} \pm u_D \varrho(\pm 1) \geq 0. \quad (2.16)$$

Clearly, (2.16) is always satisfied for (2.11)(iii), while for $u_D < 0$ it is sufficient to require $\varrho(1) = 0$, e.g. by choosing (2.11)(ii). A major advantage of (2.11)(ii) over (2.11)(iii) is that for the former it will be possible to derive almost linear finite element approximations that are unconditionally stable. The corresponding unconditionally stable schemes for the nonlinear shape function (2.11)(iii), on the other hand, turn out to be more nonlinear. Conversely, if $u_D > 0$, then only $\varrho(-1) = 0$ is needed in order to satisfy (2.16). The natural analogue for (2.11)(ii) in this situation is then

$$\varrho(s) = \frac{1}{2} (1 + s), \quad (2.17)$$

and once again it is possible to derive almost linear finite element approximations that are unconditionally stable for this choice of ϱ .

Finally we note that the quartic potential (2.2) is often preferred in applications because the discretized equations can then be solved with smooth solution methods, such as the Newton method. However, the quartic potential has the disadvantage that a priori it cannot be guaranteed that $|\varphi| \leq 1$ at all times, and in practice it can in general be observed that discretizations of φ exceed the interval $[-1, 1]$. Hence from a practical and from a numerical analysis point of view it is preferable to use the obstacle potential (2.3). Here we note that the discretized equations, which feature variational inequalities, can be efficiently solved with a variety of modern solution methods; see e.g. Barrett *et al.* (2004); Gräser and Kornhuber (2007); Bañas and Nürnberg (2008, 2009a); Blank *et al.* (2011); Hintermüller *et al.* (2011); Gräser *et al.* (2012).

2.3 Anisotropies

In this paper, we will only consider smooth and convex anisotropies, i.e. they satisfy

$$\gamma'(p) \cdot q \leq \gamma(q) \quad \forall p \in \mathbb{R}^d \setminus \{0\}, q \in \mathbb{R}^d, \quad (2.18)$$

which, on recalling (1.2), is equivalent to

$$\gamma(p) + \gamma'(p) \cdot (q - p) \leq \gamma(q) \quad \forall p \in \mathbb{R}^d \setminus \{0\}, q \in \mathbb{R}^d. \quad (2.19)$$

It is the aim of this paper to introduce unconditionally stable finite element approximations for the phase field models (2.7a–f) and (2.10a–d), (2.12a–c). Based on earlier

work by the authors in the context of the parametric approximation of anisotropic geometric evolution equations Barrett *et al.* (2008a,b), the crucial idea here is to restrict the class of anisotropies under consideration. The special structure of the chosen anisotropies can then be exploited to develop discretizations that are stable without the need for regularization and without a restriction on the time step size.

In particular, the class of anisotropies that we will consider in this paper is given by

$$\gamma(p) = \left(\sum_{\ell=1}^L [\gamma_\ell(p)]^r \right)^{\frac{1}{r}}, \quad \gamma_\ell(p) := [p \cdot G_\ell p]^{\frac{1}{2}}, \quad \forall p \in \mathbb{R}^d, \quad r \in [1, \infty), \quad (2.20)$$

where $G_\ell \in \mathbb{R}^{d \times d}$, for $\ell = 1 \rightarrow L$, are symmetric and positive definite matrices. This class of anisotropies has been previously considered by the authors in Barrett *et al.* (2008b, 2010b). We remark that anisotropies of the form (2.20) are always strictly convex norms. In particular, they satisfy (2.19). However, despite this seemingly restrictive choice, it is possible with (2.20) to model and approximate a wide variety of anisotropies that are relevant in materials science. For the sake of brevity, we refer to the exemplary Wulff shapes in the authors' previous papers Barrett *et al.* (2008a,b, 2010c,b,a, 2012a). We remark that in the case $r = 1$ all of the numerical schemes introduced in Section 3, below, will feature no additional nonlinearities compared to the isotropic case (1.3). In particular, the finite element approximation in Section 3.1 for the obstacle potential (2.3) will feature only linear equations and linear variational inequalities; see also Barrett *et al.* (2012c). Finally, we note that in the two-dimensional case ($d = 2$), the anisotropies (2.20) with the choice $r = 1$ adequately approximate most relevant anisotropies. However, in the three-dimensional setting ($d = 3$), it is often necessary to use $r > 1$ in (2.20) in order to model a chosen anisotropy. See Barrett *et al.* (2008b) for more details.

In the following, we establish some crucial results for anisotropies of the form (2.20). Note that for γ satisfying (2.20) it holds that

$$A'(p) = \gamma(p) \gamma'(p), \quad \text{where} \quad \gamma'(p) = \sum_{\ell=1}^L \left[\frac{\gamma_\ell(p)}{\gamma(p)} \right]^{r-1} \gamma'_\ell(p) \quad \forall p \in \mathbb{R}^d \setminus \{0\}. \quad (2.21)$$

For later use we recall the elementary identity

$$2y(y-z) = y^2 - z^2 + (y-z)^2. \quad (2.22)$$

Moreover, from now on we use the convention that

$$\frac{\gamma_\ell(p)}{\gamma(p)} := 1 \quad \text{if} \quad p = 0, \quad \ell = 1 \rightarrow L. \quad (2.23)$$

LEMMA. 2.2. *Let γ be of the form (2.20). Then it holds that*

$$\gamma(p) \leq L^{\frac{1}{r(r+1)}} \left(\sum_{\ell=1}^L [\gamma_\ell(p)]^{r+1} \right)^{\frac{1}{r+1}} \quad \forall p \in \mathbb{R}^d. \quad (2.24)$$

Moreover, γ is convex and the anisotropic operator A satisfies

$$A'(p) \cdot (p - q) \geq \gamma(p) [\gamma(p) - \gamma(q)] \quad \forall p \in \mathbb{R}^d \setminus \{0\}, q \in \mathbb{R}^d, \quad (2.25)$$

$$A(p) \leq \frac{1}{2} \gamma(q) \sum_{\ell=1}^L \left[\frac{\gamma_\ell(p)}{\gamma(p)} \right]^{r-1} [\gamma_\ell(q)]^{-1} [\gamma_\ell(p)]^2 \quad \forall p \in \mathbb{R}^d, q \in \mathbb{R}^d \setminus \{0\}, \quad (2.26)$$

where in (2.26) we recall the convention (2.23).

Proof. It follows from a Hölder inequality that

$$[\gamma(p)]^r \leq L^{\frac{1}{r+1}} \left(\sum_{\ell=1}^L [\gamma_\ell(p)]^{r+1} \right)^{\frac{r}{r+1}} \quad \forall p \in \mathbb{R}^d,$$

which immediately yields the desired result (2.24). Next we prove (2.18). It follows from (2.21), a Cauchy–Schwarz and a Hölder inequality that

$$\begin{aligned} \gamma'(p) \cdot q &= \sum_{\ell=1}^L \left[\frac{\gamma_\ell(p)}{\gamma(p)} \right]^{r-1} [\gamma_\ell(p)]^{-1} (G_\ell p) \cdot q \leq \sum_{\ell=1}^L \left[\frac{\gamma_\ell(p)}{\gamma(p)} \right]^{r-1} \gamma_\ell(q) \\ &\leq \left(\sum_{\ell=1}^L \left[\frac{\gamma_\ell(p)}{\gamma(p)} \right]^r \right)^{\frac{r-1}{r}} \left(\sum_{\ell=1}^L [\gamma_\ell(q)]^r \right)^{\frac{1}{r}} = \gamma(q) \quad \forall p \in \mathbb{R}^d \setminus \{0\}, q \in \mathbb{R}^d. \end{aligned}$$

Together with (1.2) this implies (2.19), i.e. γ is convex. Multiplying (2.19) with $\gamma(p)$ yields the desired result (2.25). Moreover, we have from a Hölder inequality that

$$\begin{aligned} [\gamma(p)]^r &= \sum_{\ell=1}^L [\gamma_\ell(q)]^{\frac{r}{r+1}} \frac{[\gamma_\ell(p)]^r}{[\gamma_\ell(q)]^{\frac{r}{r+1}}} \leq \left(\sum_{\ell=1}^L [\gamma_\ell(q)]^r \right)^{\frac{1}{r+1}} \left(\sum_{\ell=1}^L \frac{[\gamma_\ell(p)]^{r+1}}{\gamma_\ell(q)} \right)^{\frac{r}{r+1}} \\ \Rightarrow [\gamma(p)]^{r+1} &\leq \gamma(q) \sum_{\ell=1}^L [\gamma_\ell(p)]^{r+1} [\gamma_\ell(q)]^{-1} \quad \forall p \in \mathbb{R}^d, q \in \mathbb{R}^d \setminus \{0\}. \end{aligned}$$

This immediately yields the desired result (2.26), on recalling (2.5). \square

Our aim now is to replace the highly nonlinear operator $A'(p) : \mathbb{R}^d \rightarrow \mathbb{R}^d$ in (2.21) with an almost linear approximation (linear for $r = 1$) that still maintains the crucial monotonicity property (2.25). It turns out that a natural linearization is already given in (2.21). In particular, we let

$$B_r(q, p) := \begin{cases} \gamma(q) \sum_{\ell=1}^L \left[\frac{\gamma_\ell(p)}{\gamma(p)} \right]^{r-1} [\gamma_\ell(q)]^{-1} G_\ell & q \neq 0, \\ L^{\frac{1}{r}} \sum_{\ell=1}^L \left[\frac{\gamma_\ell(p)}{\gamma(p)} \right]^{r-1} G_\ell & q = 0, \end{cases} \quad \forall p \in \mathbb{R}^d, \quad (2.27)$$

where in the case $p = 0$ we recall (2.23). For later use we note for $q \in \mathbb{R}^d$ that

$$B_1(q, p) = B_1(q, 0) =: B_1(q) \quad \forall p \in \mathbb{R}^d. \quad (2.28)$$

Clearly it holds that

$$B_r(p, p)p = A'(p) \quad \forall p \in \mathbb{R}^d \setminus \{0\},$$

and it turns out that approximating $A'(p)$ with $B_r(q, p)p$ maintains the monotonicity property (2.25).

LEMMA. 2.3. *Let γ be of the form (2.20). Then it holds that*

$$[B_r(q, p)p] \cdot (p - q) \geq \gamma(p) [\gamma(p) - \gamma(q)] \quad \forall p, q \in \mathbb{R}^d. \quad (2.29)$$

Proof. If $p = 0$ then (2.29) trivially holds. Now let $p \in \mathbb{R}^d \setminus \{0\}$. If $q \neq 0$ it holds, on recalling (2.26), that

$$\begin{aligned} [B_r(q, p)p] \cdot (p - q) &= \gamma(q) \sum_{\ell=1}^L \left[\frac{\gamma_\ell(p)}{\gamma(p)} \right]^{r-1} [\gamma_\ell(q)]^{-1} (p - q) \cdot G_\ell p \\ &\geq \gamma(q) \sum_{\ell=1}^L \left[\frac{\gamma_\ell(p)}{\gamma(p)} \right]^{r-1} \gamma_\ell(p) ([\gamma_\ell(q)]^{-1} \gamma_\ell(p) - 1) \\ &= \gamma(q) \sum_{\ell=1}^L \left[\frac{\gamma_\ell(p)}{\gamma(p)} \right]^{r-1} [\gamma_\ell(q)]^{-1} [\gamma_\ell(p)]^2 - \gamma(q) \gamma(p) \geq \gamma(p) [\gamma(p) - \gamma(q)]. \end{aligned}$$

If $q = 0$, on the other hand, then it follows from (2.24) that

$$[B_r(q, p)p] \cdot (p - q) = [B_r(0, p)p] \cdot p = L^{\frac{1}{r}} [\gamma(p)]^{1-r} \sum_{\ell=1}^L [\gamma_\ell(p)]^{r+1} \geq [\gamma(p)]^2.$$

□

COROLLARY. 2.4. *Let γ be of the form (2.20). Then it holds that*

$$[B_r(q, p)p] \cdot (p - q) \geq A(p) - A(q) \quad \forall p, q \in \mathbb{R}^d. \quad (2.30)$$

Proof. The desired result follows immediately from Lemma 2.3 on noting the elementary identity (2.22). □

3 Finite element approximations

Let Ω be a polyhedral domain and let $\{\mathcal{T}^h\}_{h>0}$ be a family of partitionings of Ω into disjoint open simplices σ with $h_\sigma := \text{diam}(\sigma)$ and $h := \max_{\sigma \in \mathcal{T}^h} h_\sigma$, so that $\overline{\Omega} = \cup_{\sigma \in \mathcal{T}^h} \overline{\sigma}$. Associated with \mathcal{T}^h is the finite element space

$$S^h := \{\chi \in C(\overline{\Omega}) : \chi|_\sigma \text{ is linear } \forall \sigma \in \mathcal{T}^h\} \subset H^1(\Omega).$$

Let J be the set of nodes of \mathcal{T}^h and $\{p_j\}_{j \in J}$ the coordinates of these nodes. Let $\{\chi_j\}_{j \in J}$ be the standard basis functions for S^h ; that is $\chi_j \in S^h$ and $\chi_j(p_i) = \delta_{ij}$ for all $i, j \in J$. We introduce $\pi^h : C(\bar{\Omega}) \rightarrow S^h$, the interpolation operator, such that $(\pi^h \eta)(p_j) = \eta(p_j)$ for all $j \in J$. A discrete semi-inner product on $C(\bar{\Omega})$ is then defined by

$$(\eta_1, \eta_2)^h := \int_{\Omega} \pi^h(\eta_1(x) \eta_2(x)) \, dx$$

with the induced discrete semi-norm given by $|\eta|_h := [(\eta, \eta)^h]^{\frac{1}{2}}$, for $\eta \in C(\bar{\Omega})$. We extend these definitions to functions that are piecewise continuous on \mathcal{T}^h in the usual way, i.e. by setting

$$(\eta_1, \eta_2)^h := \sum_{\sigma \in \mathcal{T}^h} (\eta_1, \eta_2)_{\sigma}^h,$$

where

$$(\eta_1, \eta_2)_{\sigma}^h := \frac{|\sigma|}{d+1} \sum_{k=0}^d (\eta_1 \eta_2)((p_{j_k})^-),$$

with $\{p_{j_k}\}_{k=0}^d$ denoting the vertices of σ , and where we define $\eta((p_{j_k})^-) := \lim_{\sigma \ni q \rightarrow p_{j_k}} \eta(q)$, $k = 0 \rightarrow d$.

We introduce also

$$\begin{aligned} K^h &:= \{\chi \in S^h : |\chi| \leq 1 \text{ in } \Omega\} \subset K := \{\eta \in H^1(\Omega) : |\eta| \leq 1 \text{ a.e. in } \Omega\}, \\ S_0^h &:= \{\chi \in S^h : \chi = 0 \text{ on } \partial_D \Omega\} \quad \text{and} \quad S_D^h := \{\chi \in S^h : \chi = \pi^h u_D \text{ on } \partial_D \Omega\}, \end{aligned}$$

where in the definition of S_D^h we allow for $u_D \in H^{\frac{1}{2}}(\partial_D \Omega) \cap C(\overline{\partial_D \Omega})$.

In addition to \mathcal{T}^h , let $0 = t_0 < t_1 < \dots < t_{N-1} < t_N = T$ be a partitioning of $[0, T]$ into possibly variable time steps $\tau_n := t_n - t_{n-1}$, $n = 1 \rightarrow N$. We set $\tau := \max_{n=1 \rightarrow N} \tau_n$.

In the following we will present stable finite element approximations for the phase field model (2.10a–d), (2.12a–c) for the obstacle potential (2.3) and for the case of a smooth potential such as (2.2), respectively. In order to obtain stable approximations, the three nonlinearities arising in (2.12a) from $\varrho(\varphi)$, from $A'(\nabla \varphi)$ and from $\Psi'(\varphi)$ need to be discretized appropriately in time. Here the discretization of $A'(\nabla \varphi)$ induced by Corollary 2.4 is novel, and is one of the main contributions of this paper. The employed splitting of $\Psi'(\varphi)$ into implicit/explicit time discretizations according to a convex/concave splitting of Ψ , on the other hand, is standard; see e.g. Elliott and Stuart (1993); Barrett *et al.* (1999). We employ the same idea to the splitting of $\varrho(\varphi)$, for which we now introduce some notation. A similar notation will be used in Section 3.2 for the splitting of $\Psi'(\varphi)$ in the case of a smooth potential Ψ .

Let $\varrho^{\pm} \in C^1(\mathbb{R})$ such that $\varrho(s) = \varrho^+(s) + \varrho^-(s)$. In our finite element schemes ϱ^+ will play the role of the implicit part of the approximation of ϱ , while ϱ^- corresponds to the explicit part. We now define

$$\widehat{\varrho}(s_0, s_1) := \varrho^+(s_1) + \varrho^-(s_0) \quad \forall s_0, s_1 \in \mathbb{R}, \quad (3.1)$$

as well as $P^\pm(s) := \int_{-1}^s \varrho^\pm(y) dy$. Of particular interest will be splittings such that

$$\pm u_D (\varrho^\pm)'(s) \leq 0 \quad \forall s \leq \frac{2}{\sqrt{3}}. \quad (3.2)$$

If $u_D < 0$, then (3.2) enforces $P^+(s)$ to be convex for $s \leq \frac{2}{\sqrt{3}}$, while $P^-(s)$ is concave over the same region. Possible splittings satisfying (3.2) for the shape functions in (2.11) are then given by

$$\begin{aligned} \text{(i)} \quad & \varrho^+(s) = 0, \quad \varrho^-(s) = \varrho(s) = \frac{1}{2}, \\ \text{(ii)} \quad & \varrho^+(s) = 0, \quad \varrho^-(s) = \varrho(s) = \frac{1}{2}(1-s), \\ \text{(iii)} \quad & \varrho^+(s) = \frac{3}{2}s, \quad \varrho^-(s) = \varrho(s) - \frac{3}{2}s = \frac{15}{16}(s^4 - 2s^2 - \frac{8}{5}s + 1). \end{aligned} \quad (3.3)$$

The fact that the splitting (3.3)(iii) satisfies (3.2) follows from the observation that in that case $\max_{s \leq \frac{2}{\sqrt{3}}} \varrho'(s) = \varrho'(\frac{2}{\sqrt{3}}) = \frac{15}{16} \frac{8}{\sqrt{27}} < \frac{3}{2}$. Note that the above splittings were chosen such that the implicit part of the approximation of ϱ is as simple as possible. If $u_D > 0$, on the other hand, then swapping the roles of ϱ^\pm in (3.3) will satisfy (3.2). However, as the implicit parts ϱ^+ are then unnecessarily nonlinear in the cases (2.11)(ii) and (2.11)(iii), it is more convenient, on recalling (2.17), to use the splittings

$$\begin{aligned} \text{(ii)} \quad & \varrho^+(s) = 0, \quad \varrho^-(s) = \varrho(s) = \frac{1}{2}(1+s), \\ \text{(iii)} \quad & \varrho^+(s) = -\frac{3}{2}s, \quad \varrho^-(s) = \varrho(s) + \frac{3}{2}s = \frac{15}{16}(s^4 - 2s^2 + \frac{8}{5}s + 1), \end{aligned} \quad (3.4)$$

which will then satisfy

$$\pm u_D (\varrho^\pm)'(s) \leq 0 \quad \forall s \geq -\frac{2}{\sqrt{3}}. \quad (3.5)$$

3.1 The obstacle potential

We then consider the following fully practical finite element approximation for (2.10a–d), (2.12a–c) in the case of the obstacle potential (2.3). This approximation is an adaptation of the scheme from Elliott and Gardiner (1996) which, with the help of Corollary 2.4, can be shown to be stable. Let $\Phi^0 \in K^h$ be an approximation of $\varphi_0 \in K$, e.g. $\Phi^0 = \pi^h \varphi_0$ for $\varphi_0 \in C(\bar{\Omega})$. Similarly, if $\vartheta > 0$ let $W^0 \in S_D^h$ be an approximation of u_0 . Then, for $n \geq 1$, find $(\Phi^n, W^n) \in K^h \times S_D^h$ such that

$$\begin{aligned} \vartheta \left(\frac{W^n - W^{n-1}}{\tau_n}, \chi \right)^h + \lambda \left(\widehat{\varrho}(\Phi^{n-1}, \Phi^n) \frac{\Phi^n - \Phi^{n-1}}{\tau_n}, \chi \right)^h + (\pi^h[b(\Phi^{n-1})] \nabla W^n, \nabla \chi) = 0 \\ \forall \chi \in S_0^h, \end{aligned} \quad (3.6a)$$

$$\begin{aligned} \varepsilon \frac{\rho}{\alpha} \left(\mu(\nabla \Phi^{n-1}) \frac{\Phi^n - \Phi^{n-1}}{\tau_n}, \chi - \Phi^n \right)^h + \varepsilon (B_r(\nabla \Phi^{n-1}, \nabla \Phi^n) \nabla \Phi^n, \nabla [\chi - \Phi^n]) \\ \geq \left(c_\Psi \frac{a}{\alpha} \widehat{\varrho}(\Phi^{n-1}, \Phi^n) W^n + \varepsilon^{-1} \Phi^{n-1}, \chi - \Phi^n \right)^h \quad \forall \chi \in K^h. \end{aligned} \quad (3.6b)$$

The main differences between (3.6a,b) for $\varrho^+ = 0$, so that $\widehat{\varrho}(\Phi^{n-1}, \Phi^n) = \varrho(\Phi^{n-1})$, and the basic scheme in Elliott and Gardiner (1996, Eqs. (3.1), (3.2)) are our novel approximation

of $A'(\nabla \varphi)$ in (3.6b) and the fact that we evaluate the discrete temperature on the new time level W^n in (3.6b). The latter implies that the system (3.6a,b) is coupled, and this is needed in order to derive a stability bound, see Theorem 3.6, below. We stress that there is no stability result for the scheme Elliott and Gardiner (1996, Eqs. (3.1), (3.2)). In addition, we allow for the splitting $\varrho = \varrho^+ + \varrho^-$, so that unconditional stability can still be shown for nonlinear functions ϱ .

Let

$$\mathcal{E}_\gamma^h(W, \Phi) = \frac{\vartheta}{2} |W - u_D|_h^2 + \frac{\lambda \alpha}{a} \frac{1}{c_\Psi} \left[\frac{1}{2} \varepsilon |\gamma(\nabla \Phi)|_0^2 + \varepsilon^{-1} (\Psi(\Phi), 1)^h \right],$$

and define

$$\mathcal{F}_\gamma^h(W, \Phi) = \mathcal{E}_\gamma^h(W, \Phi) - \lambda u_D (P(\Phi), 1)^h$$

for all $W, \Phi \in S^h$, as the natural discrete analogue of the energy appearing in (2.13). We can then show that the solutions to (3.6a,b) satisfy a discrete analogue of (2.13).

We begin with considerations for the almost linear scheme (3.6a,b) with $\varrho^+ = 0$ and $r = 1$.

LEMMA. 3.1. *Let γ be of the form (2.20) with $r = 1$, let $\varrho^+ = 0$ and let $u_D \in \mathbb{R}$. Then there exists a solution $(\Phi^n, W^n) \in K^h \times S_D^h$ to (3.6a,b) and Φ^n, W^n are unique up to additive constants. If $\rho + (|\varrho(\Phi^{n-1})|, 1)^h + |(\Phi^{n-1}, 1)| > 0$, then Φ^n is unique. If $\vartheta > 0$ or $\partial_N \Omega \neq \partial \Omega$ then W^n is unique if Φ^n is unique. If $\vartheta = 0$ and $\partial_N \Omega = \partial \Omega$, and if Φ^n is unique, then W^n is unique if there exists a $j \in J$ such that $|\Phi^n(p_j)| < 1$ and $\varrho(\Phi^{n-1}(p_j)) \neq 0$.*

Proof. The proof follows the ideas in Barrett *et al.* (1999), see also Blowey and Elliott (1992). At first we assume that $\partial_N \Omega \neq \partial \Omega$ or that $\vartheta > 0$, so that $\mathcal{G}^h : S^h \rightarrow S_0^h$ such that

$$(\pi^h[b(\Phi^{n-1})] \nabla [\mathcal{G}^h v^h], \nabla \eta) + \frac{\vartheta}{\tau_n} (\mathcal{G}^h v^h, \eta)^h = (v^h, \eta)^h \quad \forall \eta \in S_0^h, \quad v^h \in S^h \quad (3.7)$$

is clearly well-defined, on recalling that

$$b(s) \geq \min\{\mathcal{K}_+, \mathcal{K}_-\} > 0 \quad \forall s \in [-1, 1].$$

Moreover, it follows from (3.6a) and (3.7) that

$$W^n - u_D = \mathcal{G}^h \left[\frac{\vartheta}{\tau_n} (W^{n-1} - u_D) - \lambda \pi^h \left[\widehat{\varrho}(\Phi^{n-1}, \Phi^n) \frac{\Phi^n - \Phi^{n-1}}{\tau_n} \right] \right]. \quad (3.8)$$

Substituting (3.8) into (3.6b), and noting (3.7) with $v^h = \pi^h[\widehat{\varrho}(\Phi^{n-1}, \Phi^n)(\chi - \Phi^n)]$ and $\eta = \mathcal{G}^h \pi^h[\widehat{\varrho}(\Phi^{n-1}, \Phi^n)(\Phi^n - \Phi^{n-1})]$ yields that

$$\begin{aligned} & \frac{\lambda c_\Psi a}{\alpha \tau_n} \left\{ (\pi^h[b(\Phi^{n-1})] \nabla [\mathcal{G}^h \pi^h[\widehat{\varrho}(\Phi^{n-1}, \Phi^n)(\Phi^n - \Phi^{n-1})]], \nabla [\mathcal{G}^h \pi^h[\widehat{\varrho}(\Phi^{n-1}, \Phi^n)(\chi - \Phi^n)]]) \right. \\ & \quad + \frac{\vartheta}{\tau_n} (\mathcal{G}^h \pi^h[\widehat{\varrho}(\Phi^{n-1}, \Phi^n)(\Phi^n - \Phi^{n-1})], \mathcal{G}^h \pi^h[\widehat{\varrho}(\Phi^{n-1}, \Phi^n)(\chi - \Phi^n)])^h \Big\} \\ & \quad + \frac{\varepsilon \rho}{\alpha \tau_n} (\mu(\nabla \Phi^{n-1}) \Phi^n, \chi - \Phi^n)^h + \varepsilon (B_r(\nabla \Phi^{n-1}, \nabla \Phi^n) \nabla \Phi^n, \nabla [\chi - \Phi^n]) \\ & \geq (f^h, \chi - \Phi^n)^h \quad \forall \chi \in K^h, \end{aligned} \quad (3.9a)$$

where

$$f^h := \left(\frac{\varepsilon \rho}{\alpha \tau_n} \mu(\nabla \Phi^{n-1}) + \varepsilon^{-1} \right) \Phi^{n-1} + c_\Psi \frac{a}{\alpha} \widehat{\varrho}(\Phi^{n-1}, \Phi^n) (u_D + \frac{\vartheta}{\tau_n} \mathcal{G}^h [W^{n-1} - u_D]) \quad (3.9b)$$

is piecewise continuous on \mathcal{T}^h . As we consider the case $\varrho^+ = 0$, from now on we use the fact that $\widehat{\varrho}(\Phi^{n-1}, \Phi^n) = \varrho(\Phi^{n-1})$. We recall from (2.27) and (2.28) that $B_1(q) \in \mathbb{R}^{d \times d}$ is symmetric and positive definite for all $q \in \mathbb{R}^d$, and hence (3.9a) are the Euler–Lagrange equations for the convex minimization problem

$$\begin{aligned} \min_{\chi \in K^h} & \left[\frac{\lambda c_\Psi a}{2 \alpha \tau_n} \left\{ (\pi^h[b(\Phi^{n-1})], |\nabla [\mathcal{G}^h \pi^h[\varrho(\Phi^{n-1})](\chi - \Phi^{n-1})]|^2) \right. \right. \\ & \left. \left. + \frac{\vartheta}{2 \tau_n} |\mathcal{G}^h \pi^h[\varrho(\Phi^{n-1})](\chi - \Phi^{n-1})|_h^2 \right\} + \frac{\varepsilon \rho}{2 \alpha \tau_n} (\mu(\nabla \Phi^{n-1}), |\chi|^2)^h \right. \\ & \left. + \frac{\varepsilon}{2} (B_1(\nabla \Phi^{n-1}) \nabla \chi, \nabla \chi) - (f^h, \chi)^h \right]. \end{aligned}$$

Therefore there exists a $\Phi^n \in K^h$ solving (3.9a) that is unique if $\rho > 0$ or $\pi^h[\varrho(\Phi^{n-1})] \neq 0 \in S^h$, and is unique up to an additive constant otherwise. In the latter case, if $(\Phi^{n-1}, 1) \neq 0$, then it immediately follows from (3.6b) that Φ^n is unique. If Φ^n is unique, then the existence of a unique $W^n \in S_D^h$, such that (Φ^n, W^n) solve (3.6a,b), follows from (3.8).

For the remainder of the proof we assume that $\partial_N \Omega = \partial \Omega$ and that $\vartheta = 0$. Then it follows immediately on choosing $\chi = 1$ in (3.6a) that $(\varrho(\Phi^{n-1}), \Phi^n)^h = (\varrho(\Phi^{n-1}), \Phi^{n-1})^h$. Taking this into account, we define $\widehat{\mathcal{G}}^h : \widehat{S}^h \rightarrow \widehat{S}^h$ such that

$$(\pi^h[b(\Phi^{n-1})] \nabla [\widehat{\mathcal{G}}^h v^h], \nabla \eta) = (v^h, \eta)^h \quad \forall \eta \in S^h, \quad v^h \in \widehat{S}^h,$$

where $\widehat{S}^h := \{\chi \in S^h : (\chi, 1) = 0\}$, and observe that (3.6a) then implies that

$$W^n = -\frac{\lambda}{\tau_n} \widehat{\mathcal{G}}^h \pi^h [\varrho(\Phi^{n-1}) (\Phi^n - \Phi^{n-1})] + \xi^n, \quad (3.10)$$

where $\xi^n \in \mathbb{R}$ is a Lagrange multiplier. It follows that (3.9a) holds with $\vartheta = 0$, with \mathcal{G}^h replaced by $\widehat{\mathcal{G}}^h$, and with K^h replaced by $\widehat{K}^h := \{\chi \in K^h : (\varrho(\Phi^{n-1}), \chi - \Phi^{n-1})^h = 0\}$. As before we can interpret this variational inequality as the Euler–Lagrange equations of a convex minimization problem, which yields the existence of a solution $\Phi^n \in \widehat{K}^h$ that is unique unless $\rho = 0$, $\pi^h[\varrho(\Phi^{n-1})] = 0$ and $(\Phi^{n-1}, 1) = 0$. Therefore, on noting (3.10), we have existence of a solution $(\Phi^n, W^n) \in K^h \times S^h$ to (3.6a,b). If Φ^n is unique, and if $|\Phi^n(p_j)| < 1$ and $\varrho(\Phi^{n-1}(p_j)) \neq 0$ for some $j \in J$ then (3.6b) holds with equality for $\chi = \chi_j$, which uniquely determines ξ^n and hence yields the uniqueness of W^n . \square

It turns out that most of the technical assumptions in Lemma 3.1 are trivially satisfied for the shape function choices in (2.11). In particular, we obtain the following result.

COROLLARY. 3.2. *Let γ be of the form (2.20) with $r = 1$, let ϱ be given by one of the choices in (2.11) or by (2.17), let $\varrho^+ = 0$ and let $u_D \in \mathbb{R}$. Then there exists a*

solution $(\Phi^n, W^n) \in K^h \times S_D^h$ to (3.6a,b) and Φ^n, W^n are unique up to additive constants. Moreover, Φ^n is unique unless ϱ is of the form (2.11)(iii), and $\rho = 0$, $(|\Phi^{n-1}|, 1)^h = |\Omega|$ and $|(\Phi^{n-1}, 1)| = 0$.

Proof. The desired results follow immediately from Lemma 3.1. \square

REMARK. 3.3. Let the assumptions of Lemma 3.1 hold and let $\partial_N \Omega \neq \partial \Omega$. Then it is easy to prove that if $\Phi^{n-1} = 1$ and $\vartheta(W^{n-1} - u_D) = 0$, and if

$$-\frac{a}{\alpha} \varrho(1) u_D \leq \frac{1}{c_\Psi} \varepsilon^{-1} \quad (3.11)$$

then the unique solution to (3.6a,b) is given by $\Phi^n = 1$ and $W^n = u_D$. If the phase field parameter ε does not satisfy (3.11), then $\Phi^n = 1$ and $W^n = u_D$ is no longer the solution to (3.6a,b). In practice it is observed that if ε does not satisfy (3.11), then the solution Φ^n exhibits a boundary layer close to $\partial \Omega$ where $\Phi^n < 1$. This artificial boundary layer is an undesired effect of the phase field approximation for the sharp interface problem (1.4a–e). In fact, and not surprisingly, (3.11) is precisely the condition on $\varrho(1)$ in (2.16). This motivates the use of shape functions with $\varrho(1) = 0$, such as (2.11)(ii) and (2.11)(iii), in practice. An obvious advantage over e.g. (2.11)(i) then is to be able to use larger values of ε , which in itself means that less fine discretization parameters may be employed.

For completeness we note that if, and only if, the condition

$$\frac{a}{\alpha} \varrho(-1) u_D \leq \frac{1}{c_\Psi} \varepsilon^{-1} \quad (3.12)$$

holds, then $\Phi^n = -1$, $W^n = u_D$ is the unique solution to (3.6a,b) for $\Phi^{n-1} = -1$ and $\vartheta(W^{n-1} - u_D) = 0$. Satisfying both (3.11) and (3.12) is equivalent to satisfying (2.16).

REMARK. 3.4. Let γ be of the form (2.20) with $r > 1$, and let the remaining assumptions of Lemma 3.1 hold. Then the highly nonlinear system (3.6a,b) for (Φ^n, W^n) is no longer continuously dependent on the variable Φ^n , recall (2.27). Due to this fact it is not possible to show existence of solutions to (3.6a,b) with the help of Brouwer's fixed point theorem. However, in practice we have no difficulties in finding solutions to the nonlinear system (3.6a,b), and the employed iterative solvers always converge; see Section 4.2. We recall that the same situation occurred in Barrett et al. (2008b), see Remark 3.3 there, where discretizations for anisotropic geometric evolution equations for anisotropic energies of the form (2.20) were considered for the very first time.

We now extend the existence result from Lemma 3.1 to the case of a general splitting $\varrho = \varrho^+ + \varrho^-$. On recalling from (2.16) and from Remark 3.3 that nontrivial choices of ϱ , i.e. alternatives to (2.11)(i), are only of interest when $\partial_N \Omega \neq \partial \Omega$, we consider the case $\varrho^+ \neq 0$ only in the presence of Dirichlet boundary conditions on W^n .

THEOREM. 3.5. Let γ be of the form (2.20) with $r = 1$ and let $u_D \in \mathbb{R}$. In addition let $\rho + |(\Phi^{n-1}, 1)| > 0$ or

$$(|\widehat{\varrho}(\Phi^{n-1}, \chi)|, 1)^h > 0 \quad \forall \chi \in K^h. \quad (3.13)$$

Moreover we assume that either $\varrho^+ = 0$, or $\vartheta > 0$, or $\partial_N \Omega \neq \partial \Omega$. Then there exists a solution $(\Phi^n, W^n) \in K^h \times S_D^h$ to (3.6a,b).

Proof. The desired result for the case $\varrho^+ = 0$ has been shown in Lemma 3.1. We now consider the case $\varrho^+ \neq 0$, so that either $\vartheta > 0$ or $\partial_N \Omega \neq \partial \Omega$. Then we can apply Brouwer's fixed point theorem to prove existence of a solution Φ^n as follows. Let the map $T : K^h \rightarrow K^h$ be defined such that $\Phi^{\text{new}} = T(\Phi^{\text{old}})$ is the solution of (3.9a,b) with $\widehat{\varrho}(\Phi^{n-1}, \Phi^n)$ replaced by $\widehat{\varrho}(\Phi^{n-1}, \Phi^{\text{old}})$, and with all other occurrences of Φ^n replaced by Φ^{new} . It follows from the proof of Lemma 3.1 and our assumptions that there exists a unique $\Phi^{\text{new}} \in K^h$, and the continuity of the map $\Phi^{\text{old}} \mapsto \Phi^{\text{new}} = T(\Phi^{\text{old}})$ together with the fact that K^h is compact and convex then yields the existence of a solution $\Phi^n \in K^h$ to (3.6a,b). The existence of a solution $W^n \in S_D^h$ then follows from (3.8). \square

The following stability theorem is the main result of this paper.

THEOREM. 3.6. *Let γ be of the form (2.20) and let $u_D \in \mathbb{R}$. Then it holds for a solution $(\Phi^n, W^n) \in K^h \times S_D^h$ to (3.6a,b) that*

$$\begin{aligned} \mathcal{E}_\gamma^h(W^n, \Phi^n) - u_D \lambda (\widehat{\varrho}(\Phi^{n-1}, \Phi^n), \Phi^n - \Phi^{n-1})^h + \tau_n (\pi^h[b(\Phi^{n-1})] \nabla W^n, \nabla W^n) \\ + \tau_n \frac{\lambda \rho}{a} \frac{\varepsilon}{c_\Psi} \left| [\mu(\nabla \Phi^{n-1})]^{\frac{1}{2}} \frac{\Phi^n - \Phi^{n-1}}{\tau_n} \right|_h^2 \leq \mathcal{E}_\gamma^h(W^{n-1}, \Phi^{n-1}). \end{aligned} \quad (3.14)$$

In particular, if the splitting $\varrho = \varrho^+ + \varrho^-$ satisfies

$$\pm u_D (\varrho^\pm)'(s) \leq 0 \quad \forall s \in [-1, 1] \quad (3.15)$$

then it holds that

$$\begin{aligned} \mathcal{F}_\gamma^h(W^n, \Phi^n) + \tau_n (\pi^h[b(\Phi^{n-1})] \nabla W^n, \nabla W^n) + \tau_n \frac{\lambda \rho}{a} \frac{\varepsilon}{c_\Psi} \left| [\mu(\nabla \Phi^{n-1})]^{\frac{1}{2}} \frac{\Phi^n - \Phi^{n-1}}{\tau_n} \right|_h^2 \\ \leq \mathcal{F}_\gamma^h(W^{n-1}, \Phi^{n-1}). \end{aligned} \quad (3.16)$$

Proof. Choosing $\chi = W^n - u_D$ in (3.6a) and $\chi = \Phi^{n-1}$ in (3.6b) yields that

$$\begin{aligned} \vartheta (W^n - W^{n-1}, W^n - u_D)^h + \lambda (\widehat{\varrho}(\Phi^{n-1}, \Phi^n) [\Phi^n - \Phi^{n-1}], W^n - u_D)^h \\ + \tau_n (\pi^h[b(\Phi^{n-1})] \nabla W^n, \nabla W^n) = 0, \end{aligned} \quad (3.17a)$$

$$\begin{aligned} \varepsilon \frac{\rho}{\alpha} \tau_n^{-1} (\mu(\nabla \Phi^{n-1}) \Phi^n - \Phi^{n-1}, \Phi^{n-1} - \Phi^n)^h + \varepsilon (B_r(\nabla \Phi^{n-1}, \nabla \Phi^n) \nabla \Phi^n, \nabla [\Phi^{n-1} - \Phi^n]) \\ \geq \left(c_\Psi \frac{a}{\alpha} \widehat{\varrho}(\Phi^{n-1}, \Phi^n) W^n + \varepsilon^{-1} \Phi^{n-1}, \Phi^{n-1} - \Phi^n \right)^h. \end{aligned} \quad (3.17b)$$

It follows from (3.17a,b), on recalling (2.22) and (2.30), that

$$\begin{aligned} \frac{1}{2} \varepsilon |\gamma(\nabla \Phi^n)|_0^2 - \frac{1}{2} \varepsilon^{-1} |\Phi^n|_h^2 + \frac{\vartheta}{2} \frac{a}{\lambda a} c_\Psi |W^n - u_D|_h^2 + \tau_n \varepsilon \frac{\rho}{\alpha} \left| [\mu(\nabla \Phi^{n-1})]^{\frac{1}{2}} \frac{\Phi^n - \Phi^{n-1}}{\tau_n} \right|_h^2 \\ - u_D \frac{a}{\alpha} c_\Psi (\widehat{\varrho}(\Phi^{n-1}, \Phi^n), \Phi^n - \Phi^{n-1})^h + \tau_n \frac{a}{\lambda \alpha} c_\Psi (\pi^h[b(\Phi^{n-1})] \nabla W^n, \nabla W^n) \\ \leq \frac{1}{2} \varepsilon |\gamma(\nabla \Phi^{n-1})|_0^2 - \frac{1}{2} \varepsilon^{-1} |\Phi^{n-1}|_h^2 + \frac{\vartheta}{2} \frac{a}{\lambda a} c_\Psi |W^{n-1} - u_D|_h^2. \end{aligned}$$

This yields the desired result (3.14) on adding the constant $\frac{1}{2}\varepsilon^{-1} \int_{\Omega} 1 \, dx$ on both sides, and then multiplying the inequality with $\frac{\lambda\alpha}{a} \frac{1}{c_{\Psi}}$. In addition, it follows from $\Phi^{n-1}, \Phi^n \in K^h$ and (3.15) that

$$\begin{aligned} u_D(\widehat{\varrho}(\Phi^{n-1}, \Phi^n), \Phi^n - \Phi^{n-1})^h &= u_D(\varrho^-(\Phi^{n-1}), \Phi^n - \Phi^{n-1})^h - u_D(\varrho^+(\Phi^n), \Phi^{n-1} - \Phi^n)^h \\ &\leq u_D(P^-(\Phi^n) - P^-(\Phi^{n-1}) + P^+(\Phi^n) - P^+(\Phi^{n-1}), 1)^h \\ &= u_D(P(\Phi^n) - P(\Phi^{n-1}), 1)^h. \end{aligned} \quad (3.18)$$

The desired result (3.16) now follows on applying (3.18) to (3.14). \square

3.2 Smooth potentials

The unconditionally stable approximation (3.6a,b) for the obstacle potential (2.3) can be easily adapted to the case of a smooth potential such as (2.2). To this end, let $\phi := \Psi'$ for an arbitrary smooth potential and let $\phi = \phi^+ + \phi^-$, with ϕ^{\pm} being the derivatives of the convex/concave parts of Ψ , i.e.

$$\pm(\phi^{\pm})'(s) \geq 0 \quad \forall s \in \mathbb{R}, \quad \Psi^{\pm} := \int_0^s \phi^{\pm}(y) \, dy. \quad (3.19a)$$

We will make the mild assumption that there exist constants $\psi_0, \psi_1, \delta > 0$ such that

$$\Psi^+(s) \geq \psi_1 |s|^{1+\delta} - \psi_0 \quad \forall s \in \mathbb{R}. \quad (3.19b)$$

For the quartic potential (2.2) the natural choices are

$$\phi^+(s) = s^3 \quad \text{and} \quad \phi^-(s) = -s, \quad (3.20)$$

so that (3.19a,b) are clearly satisfied.

As before, given $\Phi^0 \in K^h$ and, if $\vartheta > 0$, $W^0 \in S_D^h$, for $n \geq 1$, find $(\Phi^n, W^n) \in S^h \times S_D^h$ such that

$$\begin{aligned} \vartheta \left(\frac{W^n - W^{n-1}}{\tau_n}, \chi \right)^h + \lambda \left(\widehat{\varrho}_m(\Phi^{n-1}, \Phi^n) \frac{\Phi^n - \Phi^{n-1}}{\tau_n}, \chi \right)^h + (\pi^h[\widetilde{b}(\Phi^{n-1})] \nabla W^n, \nabla \chi) &= 0 \\ \forall \chi \in S_0^h, \end{aligned} \quad (3.21a)$$

$$\begin{aligned} \varepsilon \frac{\rho}{\alpha} \left(\mu(\nabla \Phi^{n-1}) \frac{\Phi^n - \Phi^{n-1}}{\tau_n}, \chi \right)^h + \varepsilon (B_r(\nabla \Phi^{n-1}, \nabla \Phi^n) \nabla \Phi^n, \nabla \chi) + \varepsilon^{-1} (\phi^+(\Phi^n), \chi)^h \\ = \left(c_{\Psi} \frac{a}{\alpha} \widehat{\varrho}_m(\Phi^{n-1}, \Phi^n) W^n - \varepsilon^{-1} \phi^-(\Phi^{n-1}), \chi \right)^h \quad \forall \chi \in S^h, \end{aligned} \quad (3.21b)$$

where in order to avoid degeneracies we have defined

$$\widetilde{b}(s) = \begin{cases} b(1) & s \geq 1, \\ b(s) & |s| \leq 1, \\ b(-1) & s \leq -1, \end{cases}$$

and where for technical reasons we have introduced

$$\widehat{\varrho}_m(s_0, s_1) := \varrho^-(s_0) + \varrho_m^+(s_1), \quad \text{where} \quad \varrho_m^+(s) := \begin{cases} \varrho^+(m) & s \geq m, \\ \varrho^+(s) & |s| \leq m, \\ \varrho^+(-m) & s \leq -m, \end{cases} \quad (3.22)$$

for some fixed parameter $m \geq 2$. We note that these modifications of (2.8) and (3.1) are such that

$$\widetilde{b}(s) \geq \min\{\mathcal{K}_+, \mathcal{K}_-\} > 0 \quad \forall s \in \mathbb{R}, \quad (3.23a)$$

$$\text{and} \quad \max_{s \in \mathbb{R}} |\widehat{\varrho}_m(s_0, s)| = \max_{|s| \leq m} |\widehat{\varrho}(s_0, s)| = C(m, s_0) \quad \forall s_0 \in \mathbb{R}. \quad (3.23b)$$

THEOREM. 3.7. *Let γ be of the form (2.20) with $r = 1$ and let $u_D \in \mathbb{R}$. If $\varrho^+ = 0$ and if ϕ^+ is strictly monotonically increasing, then there exists a unique solution $(\Phi^n, W^n) \in S^h \times S_D^h$ to (3.21a,b). If $\varrho^+ \neq 0$, and if either $\vartheta > 0$ or $\partial_N \Omega \neq \partial \Omega$, then there exists a solution $(\Phi^n, W^n) \in S^h \times S_D^h$ to (3.21a,b) if Ψ^+ satisfies the assumption (3.19b).*

Proof. The existence and uniqueness proof for the case $\varrho^+ = 0$, which is a simple modification of the proof of Lemma 3.1, is left to the reader. Note that this proof makes use of the strict monotonicity of ϕ^+ .

In order to proof existence for the case $\varrho^+ \neq 0$, we apply Brouwer's fixed point theorem. It is this part of the proof that requires the cut-off of $\widehat{\varrho}$ defined in (3.22), as well as the mild assumption (3.19b). The application of Brouwer's fixed point theorem is similar to the proof of Theorem 3.5. Setting up the map $\Phi^{\text{old}} \mapsto \Phi^{\text{new}} = T(\Phi^{\text{old}})$ analogously to the proof there, we immediately see that the map T is well-defined and continuous, where we recall that our assumptions yield that $\vartheta > 0$ or $\partial_N \Omega \neq \partial \Omega$. It remains to show that $T : Y^h \rightarrow Y^h$ for a bounded subset $Y^h \subset S^h$. To this end, on recalling (3.9a,b), we note that $\Phi^{\text{new}} \in S^h$ satisfies

$$\begin{aligned} & \frac{\lambda c_\Psi a}{\alpha \tau_n} \left\{ (\pi^h[\widetilde{b}(\Phi^{n-1})]) \nabla [\widetilde{\mathcal{G}}^h \pi^h[\widehat{\varrho}_m(\Phi^{n-1}, \Phi^{\text{old}})(\Phi^{\text{new}} - \Phi^{n-1})]], \nabla [\widetilde{\mathcal{G}}^h \pi^h[\widehat{\varrho}_m(\Phi^{n-1}, \Phi^{\text{old}}) \chi]] \right\} \\ & + \frac{\vartheta}{\tau_n} (\widetilde{\mathcal{G}}^h \pi^h[\widehat{\varrho}_m(\Phi^{n-1}, \Phi^{\text{old}})(\Phi^{\text{new}} - \Phi^{n-1})], \widetilde{\mathcal{G}}^h \pi^h[\widehat{\varrho}_m(\Phi^{n-1}, \Phi^{\text{old}}) \chi])^h \Big\} \\ & + \frac{\varepsilon \rho}{\alpha \tau_n} (\mu(\nabla \Phi^{n-1}) \Phi^{\text{new}}, \chi)^h + \varepsilon (B_1(\nabla \Phi^{n-1}) \nabla \Phi^{\text{new}}, \nabla \chi) + \varepsilon^{-1} (\phi^+(\Phi^{\text{new}}), \chi)^h \\ & = (g^h, \chi)^h \quad \forall \chi \in S^h, \end{aligned}$$

where $g^h := \frac{\varepsilon \rho}{\alpha \tau_n} \mu(\nabla \Phi^{n-1}) \Phi^{n-1} - \varepsilon^{-1} \phi^-(\Phi^{n-1}) + c_\Psi \frac{a}{\alpha} \widehat{\varrho}_m(\Phi^{n-1}, \Phi^{\text{old}})(u_D + \frac{\vartheta}{\tau_n} \widetilde{\mathcal{G}}^h[W^{n-1} - u_D])$, and where $\widetilde{\mathcal{G}}^h$ is defined by (3.7) with b replaced by \widetilde{b} . These are the Euler–Lagrange equations for the convex minimization problem

$$\min_{\chi \in S^h} [J(\chi) - (g^h, \chi)^h], \quad (3.24a)$$

where

$$\begin{aligned}
J(\chi) := & \frac{\lambda c_\Psi a}{2\alpha\tau_n} \left\{ (\pi^h[\tilde{b}(\Phi^{n-1})], |\nabla[\tilde{\mathcal{G}}^h \pi^h[\widehat{\varrho}_m(\Phi^{n-1}, \Phi^{\text{old}})(\chi - \Phi^{n-1})]]|^2) \right. \\
& + \frac{\vartheta}{2\tau_n} |\tilde{\mathcal{G}}^h \pi^h[\widehat{\varrho}_m(\Phi^{n-1}, \Phi^{\text{old}})(\chi - \Phi^{n-1})]|_h^2 \Big\} + \frac{\varepsilon\rho}{2\alpha\tau_n} (\mu(\nabla\Phi^{n-1}), |\chi|^2)^h \\
& + \frac{\varepsilon}{2} (B_1(\nabla\Phi^{n-1})\nabla\chi, \nabla\chi) + \varepsilon^{-1}(\Psi^+(\chi), 1)^h \quad \forall \chi \in S^h. \tag{3.24b}
\end{aligned}$$

It follows from (3.24a,b) and (3.23a,b) that

$$\varepsilon^{-1}(\Psi^+(\Phi^{\text{new}}, 1)^h - (g^h, \Phi^{\text{new}})^h \leq J(\Phi^{\text{new}}) - (g^h, \Phi^{\text{new}})^h \leq J(0) \leq C(\Phi^{n-1}). \tag{3.25}$$

Applying the elementary inequality $yz \leq \frac{1}{p}|y|^p + \frac{1}{q}|z|^q$, for $p, q \in (1, \infty)$ with $\frac{1}{p} + \frac{1}{q} = 1$, to the second term in (3.25) yields that

$$(g^h, \Phi^{\text{new}})^h \leq \frac{1}{2}\varepsilon^{-1}\psi_1(|\Phi^{\text{new}}|^{1+\delta}, 1)^h + C(\varepsilon, \delta, g^h), \tag{3.26}$$

where ψ_1 and δ are as in (3.19b). Now combining (3.25) and (3.26), on recalling the mild assumption (3.19b), yields that $(|\Phi^{\text{new}}|^{1+\delta}, 1)^h \leq C$ for some constant $C > 0$ independent of Φ^{old} , i.e.

$$(|T(\chi)|^{1+\delta}, 1)^h \leq C \quad \forall \chi \in S^h. \tag{3.27}$$

Hence $T : Y^h \rightarrow Y^h$ for a bounded subset $Y^h \subset S^h$, and so Brouwer's fixed point theorem yields the existence of a solution Φ^n to (3.21a,b). The existence of a solution $W^n \in S_D^h$ then follows from (3.8) with \mathcal{G}^h replaced by $\tilde{\mathcal{G}}^h$ and with $\widehat{\varrho}$ replaced by $\widehat{\varrho}_m$. \square

We stress that the cut-off introduced in (3.22) is for technical reasons only. If a solution $(\Phi^n, W^n) \in S^h \times S_D^h$ to (3.21a,b) is such that $|\Phi^n| \leq m$, then clearly $(\Phi^n, W^n) \in S^h \times S_D^h$ also solves (3.21a,b) with $\widehat{\varrho}_m$ replaced by $\widehat{\varrho}$. In practice, this is always the case for m chosen sufficiently large. Hence for practical implementations, only (3.21a,b) with $\widehat{\varrho}_m$ replaced by $\widehat{\varrho}$ needs to be considered.

COROLLARY. 3.8. *Let γ be of the form (2.20) with $r = 1$ and let $u_D \in \mathbb{R}$. Let Ψ be given by (2.2) and let (3.20) hold. Let ϱ and its splitting be defined by one of the choices in (3.3) or (3.4). Then there exists a solution $(\Phi^n, W^n) \in S^h \times S_D^h$ to (3.21a,b) unless in cases (3.3)(iii) and (3.4)(iii) it holds that $\vartheta = 0$ and $\partial_N\Omega = \partial\Omega$. Moreover, (Φ^n, W^n) is unique for the choices (3.3)(i), (3.3)(ii) and (3.4)(ii).*

Proof. The desired results follow immediately from Theorem 3.7 on noting that (3.20) satisfies the assumptions on ϕ^+ and Ψ^+ stated there. \square

REMARK. 3.9. *Similarly to Remark 3.3, the following observation holds for the scheme (3.21a,b) when $r = 1$, $\varrho^+ = 0$, $u_D \in \mathbb{R}$ and ϕ^+ is strictly monotonically increasing. Then, if $\Phi^{n-1} = 1$ and $\vartheta(W^{n-1} - u_D) = 0$, then the unique solution to (3.21a,b) is given by $\Phi^n = 1$ and $W^n = u_D$ if and only if*

$$u_D \varrho(1) = 0. \tag{3.28}$$

For nonzero u_D this is precisely the necessary condition for $G(s)$ in (2.15) to have a local minimum at $s = 1$. In practice, if the condition (3.28) is violated, then for certain values of u_D and ε artificial boundary layers develop. This undesired effect for the choice (2.11)(i) once again motivates the use of the alternatives (2.11)(ii) and (2.11)(iii) in practice.

The following stability result is the natural analogue of Theorem 3.6 for the case of a smooth potential Ψ .

THEOREM. 3.10. *Let γ be of the form (2.20) and let $u_D \in \mathbb{R}$. Then it holds that a solution $(\Phi^n, W^n) \in S^h \times S_D^h$ to (3.21a,b) satisfies (3.14) with b replaced by \tilde{b} , and with $\hat{\varrho}$ replaced by $\hat{\varrho}_m$. In particular, if the splitting $\varrho = \varrho^+ + \varrho^-$ satisfies (3.2), and if*

$$\Phi^{n-1} \leq \frac{2}{\sqrt{3}} \quad \text{and} \quad \Phi^n \leq \frac{2}{\sqrt{3}}, \quad (3.29a)$$

or if it satisfies (3.5), and if

$$\Phi^{n-1} \geq -\frac{2}{\sqrt{3}} \quad \text{and} \quad \Phi^n \geq -\frac{2}{\sqrt{3}}, \quad (3.29b)$$

then the solution (Φ^n, W^n) satisfies the stability bound (3.16) with b replaced by \tilde{b} .

Proof. The proof of the stability bounds, which is a simple modification of the proof of Theorem 3.6, is left to the reader. Note that the proof makes use of the splittings $\phi = \phi^+ + \phi^-$ and $\varrho = \varrho^+ + \varrho^-$, recall (3.18). \square

COROLLARY. 3.11. *Let γ be of the form (2.20) and let $u_D \in \mathbb{R}$. Then for the choices of ϱ and its splittings in (3.3)(i), (3.3)(ii) and (3.4)(ii) it holds that the unique solution $(\Phi^n, W^n) \in S^h \times S_D^h$ to (3.21a,b) satisfies the stability bound (3.16) with b replaced by \tilde{b} . For the choice (2.11)(iii), with the splittings (3.3)(iii) or (3.4)(iii), it holds that a solution $(\Phi^n, W^n) \in S^h \times S_D^h$ to (3.21a,b) satisfies the same stability bound if (3.29a) or (3.29b) hold, respectively.*

Proof. The desired results for the splittings (3.3)(i), (3.3)(ii) and (3.4)(ii), on recalling Corollary 3.8, follow from the fact that these splittings satisfy the inequalities in (3.2) for all $s \in \mathbb{R}$. The results for (2.11)(iii) follow immediately from Theorem 3.10. \square

In practice, in general, the values of Φ^n are either within the interval $[-1, 1]$, or very close to it. In our experience, for the scheme (3.21a,b) with (2.11)(iii) and with the splittings (3.3)(iii) and (3.4)(iii) for $u_D \leq 0$ and $u_D > 0$, respectively, in practice (3.29a) and (3.29b) always hold. Here we note that $\frac{2}{\sqrt{3}} \approx 1.15$.

4 Solution of the algebraic systems of equations

The system of nonlinear equations for (Φ^n, W^n) arising at each time level from the approximation (3.21a,b) can be solved with a Newton method or with a nonlinear multigrid method, see e.g. Kim *et al.* (2004).

For the remainder of this section we discuss the solution of the systems of algebraic equations for (Φ^n, W^n) arising at each time level from the approximation (3.6a,b). Adopting the obvious notation, the system (3.6a,b) can be rewritten as: Find $(\Phi^n, W^n) \in [-1, 1]^{\mathcal{J}} \times \mathbb{R}^{\mathcal{J}}$, $\mathcal{J} := \#J$, such that

$$\lambda M_\varrho(\Phi^n) \Phi^n + (\vartheta M + \tau_n A) W^n = \tilde{f}(\Phi^n) \quad (4.1a)$$

$$\begin{aligned} \varepsilon \frac{\rho}{\alpha} \tau_n^{-1} (V - \Phi^n)^T M_\mu \Phi^n + \varepsilon (V - \Phi^n)^T \mathcal{B}_r(\Phi^n) \Phi^n - c_\Psi \frac{a}{\alpha} (V - \Phi^n)^T M_\varrho(\Phi^n) W^n \\ \geq (V - \Phi^n)^T \tilde{g} \quad \forall V \in [-1, 1]^{\mathcal{J}}, \end{aligned} \quad (4.1b)$$

where M , M_μ , $M_\varrho(\eta)$, A and $\mathcal{B}_r(\eta)$, for $\eta \in S^h$, are symmetric $\mathcal{J} \times \mathcal{J}$ matrices. In the case of pure Neumann boundary conditions, (1.5)(ii), their entries are given by $M_{ij} := (\chi_i, \chi_j)^h$, $[M_\mu]_{ij} := (\mu(\nabla \Phi^{n-1}) \chi_i, \chi_j)^h$, $[M_\varrho(\eta)]_{ij} := (\hat{\varrho}(\Phi^{n-1}, \eta) \chi_i, \chi_j)^h$,

$$[\mathcal{B}_r(\eta)]_{ij} := (B_r(\nabla \Phi^{n-1}, \nabla \eta) \nabla \chi_i, \nabla \chi_j), \quad A_{ij} := (\pi^h[b(\Phi^{n-1})] \nabla \chi_i, \nabla \chi_j),$$

while the right hand sides in this case are defined as $\tilde{f}(\Phi^n) := \lambda M_\varrho(\Phi^n) \Phi^{n-1} + \vartheta M W^{n-1}$ and $\tilde{g} := \varepsilon \frac{\rho}{\alpha} \tau_n^{-1} M_\mu \Phi^{n-1} + \varepsilon^{-1} M \Phi^{n-1} \in \mathbb{R}^{\mathcal{J}}$. Of course, for the cases (1.5)(i) and (1.5)(iii) these entries need to be appropriately manipulated.

Clearly, the algebraic system (4.1a,b) can be written as a (symmetric) nonsmooth saddle point problem of the form: Find $(U, W) \in [-1, 1]^{\mathcal{J}} \times \mathbb{R}^{\mathcal{J}}$,

$$\mathcal{M}_\varrho(U) U + \mathcal{A} W = f_\varrho(U) \quad (4.2a)$$

$$(V - U)^T \mathcal{C}_r(U) U - (V - U)^T \mathcal{M}_\varrho(U) W \geq (V - U)^T g \quad \forall V \in [-1, 1]^{\mathcal{J}}, \quad (4.2b)$$

where we prefer to write the unknowns as (U, W) in place of (Φ^n, W^n) , in order to highlight the connection to discretizations of Cahn–Hilliard equations, where the former notation is standard. On recalling (2.28) and (3.1), we note that (4.2a,b) in the case $r = 1$ and $\varrho^+ = 0$ collapses to

$$\mathcal{M} U + \mathcal{A} W = f \quad (4.3a)$$

$$(V - U)^T \mathcal{C} U - (V - U)^T \mathcal{M} W \geq (V - U)^T g \quad \forall V \in [-1, 1]^{\mathcal{J}}, \quad (4.3b)$$

where $\mathcal{C} := \mathcal{C}_1(0)$, $\mathcal{M} := \mathcal{M}_\varrho(0)$ and $f := f_\varrho(0)$. Nonsmooth saddle point problems of the form (4.3a,b) are well-known from the numerical approximation of (isotropic) Cahn–Hilliard equations. Various different solution methods for the system (4.3a,b) are discussed in Barrett *et al.* (2004); Gräser and Kornhuber (2007); Bañas and Nürnberg (2008, 2009a); Blank *et al.* (2011); Hintermüller *et al.* (2011); Gräser *et al.* (2012). In the case $r = 1$ we use the solution method from Bañas and Nürnberg (2008) in order to solve (4.3a,b). In the remainder of this section we consider the case $r \geq 1$. We now state possible solution methods for the nonlinear nonsmooth saddle point problem (4.2a,b).

4.1 Nonlinear Uzawa-multigrid iteration

In what follows, we will extend the Uzawa-multigrid iteration from Bañas and Nürnberg (2008), which is based on the ideas in Gräser and Kornhuber (2007), to the highly nonlinear saddle point problem (4.2a,b). The method from Bañas and Nürnberg (2008) can

be interpreted as a primal active set method, where the approximation of the active set is driven by the current iterate W_k in (4.3b), rather than via a dual parameter as in e.g. Blank *et al.* (2011).

Given an initial iterate $(U_0, W_0) \in [-1, 1]^{\mathcal{J}} \times \mathbb{R}^{\mathcal{J}}$, for $k \geq 0$ let $U_{k+\frac{1}{2}} \in [-1, 1]^{\mathcal{J}}$ be the solution of

$$(V - U_{k+\frac{1}{2}})^T \mathcal{C}_r(U_k) U_{k+\frac{1}{2}} \geq (V - U_{k+\frac{1}{2}})^T (g + \mathcal{M}_{\varrho}(U_k) W_k) \quad \forall V \in [-1, 1]^{\mathcal{J}}. \quad (4.4a)$$

Then we define the active sets as

$$J_k^{\pm} := \{j \in J : [U_{k+\frac{1}{2}}]_j = \pm 1\} \quad \text{and let} \quad J_k = J_k^+ \cup J_k^-. \quad (4.4b)$$

Now we seek the solution $(U_{k+1}, W_{k+1}) \in \mathbb{R}^{\mathcal{J}} \times \mathbb{R}^{\mathcal{J}}$ to the linear system

$$\begin{pmatrix} \widehat{\mathcal{C}}_r(J_k, U_k) & -\widehat{\mathcal{M}}_{\varrho}(J_k, U_k) \\ \mathcal{M}_{\varrho}(U_k) & \mathcal{A} \end{pmatrix} \begin{pmatrix} U_{k+1} \\ W_{k+1} \end{pmatrix} = \begin{pmatrix} \widehat{g}(J_k^+, J_k^-) \\ f_{\varrho}(U_k) \end{pmatrix}, \quad (4.4c)$$

where, for $j \in J$,

$$[\widehat{\mathcal{C}}_r(J_k, U_k)]_{ij} = \begin{cases} \delta_{ij} & i \in J_k, \\ [\mathcal{C}_r(U_k)]_{ij} & i \in J \setminus J_k, \end{cases} \quad [\widehat{\mathcal{M}}_{\varrho}(J_k, U_k)]_{ij} = \begin{cases} 0 & i \in J_k, \\ [\mathcal{M}_{\varrho}(U_k)]_{ij} & i \in J \setminus J_k, \end{cases}$$

and

$$[\widehat{g}(J_k^+, J_k^-)]_i = \begin{cases} \pm 1 & i \in J_k^{\pm}, \\ g_i & i \in J \setminus J_k. \end{cases}$$

Now we continue the iteration (4.4a–c), until convergence is obtained, i.e. until

$$J_{k+1}^{\pm} = J_k^{\pm} \quad \text{and} \quad \max \left\{ \max_{j \in J} |[U_{k+1}]_j - [U_k]_j|, \max_{j \in J} |[W_{k+1}]_j - [W_k]_j| \right\} < tol, \quad (4.5)$$

where $tol = 10^{-8}$ is a given fixed tolerance. If a good initial guess W_0 is not available, then for $k = 0$ it can be beneficial to set $U_{\frac{1}{2}} = U_0$, rather than to employ (4.4a). Observe that since the iterates $U_{k+\frac{1}{2}}$ are only needed to define the active sets J_k^{\pm} in (4.4b), an iterative procedure to find the solution of (4.4a) can be stopped as soon as the active sets J_k^{\pm} have been found. In practice we stop the iteration as soon as two successive iterates for (4.4a) have the same active sets, which is usually the case after a few projected block Gauss–Seidel iterations. Alternatively, a monotone multigrid method could be employed to solve (4.4a), see Kornhuber (1994). The linear saddle point problems (4.4c) can be solved with a multigrid method using block Gauss–Seidel smoothers or, alternatively, with a direct solution method such as UMFPACK (Davis (2004)) or LDL (Davis (2005)), together with the sparse matrix ordering package AMD (Amestoy *et al.* (2004)). Here for the multigrid solver and the LDL factorization package, the linear system (4.4c) needs to be equivalently reformulated with a symmetric block matrix, which is easily possible. Finally, we observe that in the case $r = 1$ and $\varrho^+ = 0$, the first stopping criterion in (4.5) immediately implies the second criterion in (4.5), as then the linear system (4.4c) does not depend on the iterates U_k .

REMARK. 4.1. *In practice, in our computations, the iteration (4.4a–c) did not converge for values of $r > 3$, while it usually converged for smaller values of r . In particular, it always converged in the case $r = 1$ for the nonlinear approximation (3.6a,b) with the splitting (3.3)(iii). However, as we are interested in performing simulations for much larger values of r , e.g. $r = 9$ for ANI₉, below, we also consider a more robust solution method in the next subsection.*

4.2 Lagged fixed point iteration

In this subsection we consider a lagged fixed point iteration, where at each iteration a subproblem of the form (4.3a,b) needs to be solved.

Let $k = 0$. Given an initial iterate $(U_0, W_0) \in [-1, 1]^{\mathcal{J}} \times \mathbb{R}^{\mathcal{J}}$, we let $(U_{k+\frac{1}{2}}, W_{k+\frac{1}{2}}) \in [-1, 1]^{\mathcal{J}} \times \mathbb{R}^{\mathcal{J}}$ be the solution of

$$\mathcal{M}_{\varrho}(U_k) U_{k+\frac{1}{2}} + \mathcal{A} W_{k+\frac{1}{2}} = f_{\varrho}(U_k) \quad (4.6a)$$

$$(V - U_{k+\frac{1}{2}})^T \mathcal{C}_r(U_k) U_{k+\frac{1}{2}} - (V - U_{k+\frac{1}{2}})^T \mathcal{M}_{\varrho}(U_k) W_{k+\frac{1}{2}} \geq (V - U_{k+\frac{1}{2}})^T g \quad \forall V \in [-1, 1]^{\mathcal{J}}. \quad (4.6b)$$

On obtaining $(U_{k+\frac{1}{2}}, W_{k+\frac{1}{2}})$, we set

$$(U_{k+1}, W_{k+1}) = (1 - \mu) (U_k, W_k) + \mu (U_{k+\frac{1}{2}}, W_{k+\frac{1}{2}}), \quad (4.6c)$$

where $\mu \in (0, 1]$ is a fixed relaxation parameter. The iteration (4.6a–c) is repeated until

$$\max \left\{ \max_{j \in J} |[U_{k+1}]_j - [U_k]_j|, \max_{j \in J} |[W_{k+1}]_j - [W_k]_j| \right\} < tol.$$

In practice, the iteration (4.6a–c) always converged, provided μ was chosen sufficiently small.

5 Numerical experiments

In this section we report on numerical experiments for the proposed finite element approximations. Apart from a single computation for the approximation (3.21a,b) in the case of the quartic potential (2.2), where we employ the splitting (3.20), we will present results for the approximation (3.6a,b) for the obstacle potential (2.3) only. Our preference for the scheme (3.6a,b) over the alternative approximation (3.21a,b) stems from the fact that in the former the phase field approximation Φ^n is guaranteed to stay inside the interval $[-1, 1]$, while the latter scheme in general admits values $|\Phi^n| > 1$, which in practice is observed if e.g. a well developed interface is present. Moreover, the bulk regions for the approximation (3.6a,b) are easily identified through $\Phi^n = \pm 1$, whereas for the scheme

(3.21a,b) this is less straightforward. For the implementation of the approximations we have used the adaptive finite element toolbox ALBERTA, see Schmidt and Siebert (2005). For the approximation (3.6a,b) we employ the adaptive mesh strategy introduced in Barrett *et al.* (2004) and Bañas and Nürnberg (2008), respectively, for $d = 2$ and $d = 3$. This results in a fine mesh of uniform mesh size h_f inside the interfacial region $|\Phi^{n-1}| < 1$ and a coarse mesh of uniform mesh size h_c further away from it. Here $h_f = \frac{2H}{N_f}$ and $h_c = \frac{2H}{N_c}$ are given by two integer numbers $N_f > N_c$, where we assume from now on that $\Omega = (-H, H)^d$. In all of the experiments below we have $H = \frac{1}{2}$ with (1.5)(i), unless otherwise stated.

Throughout this section the initial data $\varphi_0 \in C(\bar{\Omega})$ is either chosen constant, $\varphi_0 = 1$, or is chosen with a well developed interface of width $\varepsilon \pi$, in which φ_0 varies smoothly and such that $\Gamma_0 = \{x \in \Omega : \varphi_0(x) = 0\}$. Details of such initial data can be found in e.g. Barrett *et al.* (2004); Bañas and Nürnberg (2009b, 2008). In general the initial interface Γ_0 is a circle/sphere of radius $R_0 \in (0, H)$ around the origin. We use $R_0 = 0.1$ unless otherwise stated. If $\vartheta > 0$, we set

$$u_0(z) = \begin{cases} 0 & |z| \leq R_0, \\ \frac{u_D}{1 - e^{R_0 - H}} (1 - e^{R_0 - |z|}) & R_0 < |z| < H, \\ u_D & |z| \geq H. \end{cases}$$

We always fix $\Phi^0 = \pi^h \varphi_0$ and, if $\vartheta > 0$, $W^0 = \pi^h u_0$.

Unless otherwise stated we always let $\varepsilon^{-1} = 16 \pi$ and $N_f = 128$, $N_c = 16$. In addition, we employ uniform time steps $\tau_n = \tau$, $n = 1 \rightarrow N$. As an indication for the computational effort that is involved in producing the simulations presented in this section, we state for each simulation an exemplary CPU time for a single-thread run on an Intel i7-860 (2.8 GHz) processor.

For the anisotropies in our numerical results we always choose among

$$\begin{aligned} \text{ANI}_1^{(\delta)}: \quad \gamma(p) &= \sum_{j=1}^d [\delta^2 |p|^2 + p_j^2 (1 - \delta^2)]^{\frac{1}{2}}, \quad \text{with } \delta > 0, \quad [r = 1, L = d], \\ \text{ANI}_2: \quad \gamma &\text{ as on the bottom of Figure 3 in Barrett } et al. (2008b), \quad [r = 1, L = 2], \\ \text{ANI}_3: \quad \gamma &\text{ as on the right of Figure 2 in Barrett } et al. (2010b), \quad [r = 1, L = 3], \\ \text{ANI}_4: \quad \gamma &\text{ as in Figure 3 in Barrett } et al. (2012b), \quad [r = 1, L = 4], \\ \text{ANI}_9: \quad \gamma &\text{ as on the right of Figure 3 in Barrett } et al. (2010b), \quad [r = 9, L = 3]. \end{aligned}$$

We remark that $\text{ANI}_1^{(\delta)}$ is a regularized l_1 -norm, so that its Wulff shape for δ small is given by a smoothed square (in 2d) or a smoothed cube (in 3d) with nearly flat sides/facets. Anisotropies with such flat sides or facets are called crystalline. Also the choices ANI_i , $i = 2 \rightarrow 4$, represent nearly crystalline anisotropies. Here the Wulff shapes are given by a smoothed cylinder, a smoothed hexagon and a smoothed hexagonal prism, respectively. The Wulff shape for the cubic anisotropy ANI_9 is given by a smoothed octahedron. Finally, we denote by ANI_k^* the anisotropies ANI_k , $k = 3 \rightarrow 4$, rotated by $\frac{\pi}{12}$ in the $x_1 - x_2$ -plane.

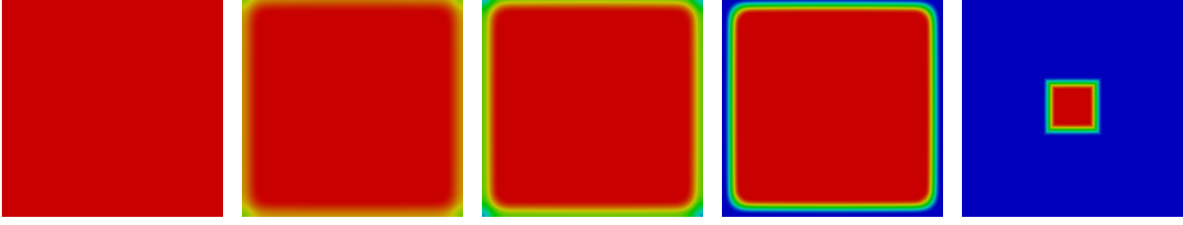


Figure 1: ($\varepsilon^{-1} = 16\pi$, $\text{ANI}_1^{(0.01)}$, (2.11)(i), $\alpha = 1$, $\rho = 10^{-3}$, $u_D = -65$, $\Omega = (-\frac{1}{2}, \frac{1}{2})^2$) Creation of a boundary layer for the scheme (3.6a,b). Snapshots of the solution at times $t = 0, 4 \times 10^{-5}, 5 \times 10^{-5}, 7 \times 10^{-5}, 10^{-3}$.

Finally, unless otherwise stated, we choose $\lambda = a = \mathcal{K}_{\pm} = 1$ and $\beta = \gamma$, where we recall (2.6).

5.1 Mullins–Sekerka in two space dimensions

In this subsection we always choose $\vartheta = 0$. We begin with an investigation into the choice of ϱ . At first we choose (2.11)(i). In order to visualize the possible onset of a boundary layer as explained in Remark 3.3 for the obstacle potential (2.3), we present a computation for (3.6a,b) with the initial data $\Phi^0 = \varphi_0 = 1$. For this experiment we use $\rho = 10^{-3}$. On setting $\alpha = 1$, the critical value for u_D in (3.11) is $-\frac{2}{c_{\Psi}}\varepsilon^{-1} = -\frac{4}{\pi}16\pi = -64$. In our numerical computations this lower bound appears to be sharp. In particular, we observe that $U^n = 1$ is a steady state whenever $u_D \geq -64$, but a boundary layer forms already for e.g. $u_D = -64 - 10^{-8}$. The same behaviour has been observed by the authors in Barrett *et al.* (2012c) for the choice $\rho = 0$. As an example for the case $\rho = 10^{-3}$ considered here, we present a run for $u_D = -65$ in Figure 1, where we can clearly see how the boundary layer develops. Note that this phenomenon is completely independent from the choice of anisotropy γ . The discretization parameters for this experiment were $N_f = N_c = 128$ and $\tau = 10^{-5}$. Note that in the presence of $\rho > 0$ we observe a convex shape in Figure 1, in contrast to the corresponding evolution in Barrett *et al.* (2012c, Fig. 4), where $\rho = 0$.

For the approximation (3.21a,b), i.e. in the case of the smooth quartic potential (2.2), we observe that the criterion (3.28) is of course not sharp, in the sense that even for values $0 > u_D \geq -41$ no boundary layer forms in practice, even though (3.28) is then violated for the shape function (2.11)(i). What happens in practice is that Φ^n attains values less than 1, without forming an interface, i.e. $\min_{x \in \Omega} \Phi^n(x) > 0$. However, for the value $u_D = -42$, with the remaining parameters fixed as in Figure 1, we do observe the creation of a boundary layer. The evolution can be seen in Figure 2. We remark that the colour range in Figure 2 is from red for 1 to blue for -1 , as in Figure 1, even though the extremal values for Φ^n during the evolution are approximately 1.03 and -1.16 , respectively. Finally, we recall that if we choose the shape functions (2.11)(ii) or (2.11)(iii) instead, then the conditions (3.11) and (3.28) yield that $\Phi^n = 1$ and $W^n = u_D$ for all $n \geq 1$ for the two schemes (3.6a,b) and (3.21a,b), respectively.

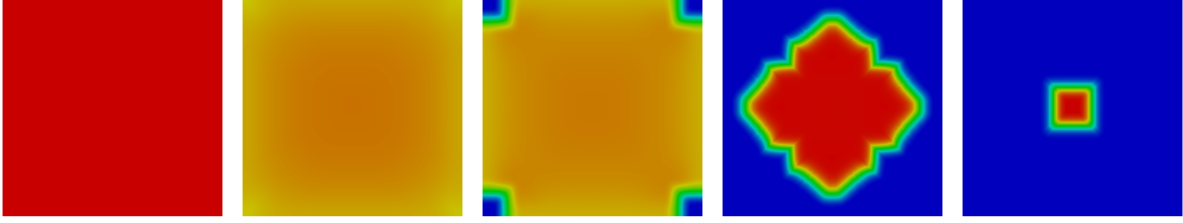


Figure 2: ($\varepsilon^{-1} = 16\pi$, $\text{ANI}_1^{(0.01)}$, (2.11)(i), $\alpha = 1$, $\rho = 10^{-3}$, $u_D = -42$, $\Omega = (-\frac{1}{2}, \frac{1}{2})^2$) Creation of a boundary layer for the scheme (3.21a,b). Snapshots of the solution at times $t = 0, 8 \times 10^{-4}, 10^{-3}, 1.5 \times 10^{-3}, 2.5 \times 10^{-3}$.

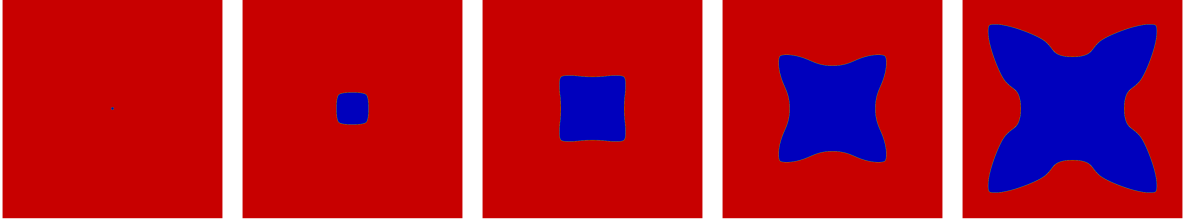


Figure 3: ($\varepsilon^{-1} = 32\pi$, $\text{ANI}_1^{(0.3)}$, (2.11)(i), $\alpha = 0.03$, $\rho = 0$, $u_D = -2$, $\Omega = (-8, 8)^2$) Snapshots of the solution at times $t = 0, 1, 3, 5, 7$. [This computation took 6 days.]

In the following experiments, we return to the initial data described previously, so that φ_0 models a circular interface of radius $R_0 = 0.1$. We also set $\rho = 0$. For convenience we recall the simulation from Barrett *et al.* (2012c, Fig. 5), so that (2.11)(i) applies. Here $H = 8$ and $\vartheta = \rho = 0$. Moreover, $u_D = -2$ and $\alpha = 0.03$; and we observe that for this choice of parameters the condition (3.11) is satisfied if we choose $\varepsilon^{-1} = 32\pi > \frac{50}{3}\pi$. A run for (3.6a,b), with the discretization parameters $N_f = 4096$, $N_c = 128$, $\tau = 10^{-4}$ and $T = 7$ is shown in Figure 3. Now the advantage of the shape function choices (2.11)(ii) and (2.11)(iii) over the simple choice (2.11)(i), as highlighted in Remark 3.3, is that for the same physical parameters a larger value of ε can be chosen. To illustrate this, we repeat the simulation from Figure 3 but now for the choices (2.11)(ii) and (2.11)(iii). This means that we can use e.g. $\varepsilon^{-1} = 8\pi$ together with the coarser discretization parameters $N_f = 1024$, $N_c = 128$ and $\tau = 10^{-3}$. The new results are shown in Figures 4 and 5, where we observe the good qualitative agreement with Figure 3. We draw particular attention to the dramatic reduction in CPU time necessary to compute the respective simulations. While a further reduction in ε^{-1} and in the discretization parameters N_f , N_c and τ^{-1} leads to even bigger gains in computation times, the larger values of ε soon lead to a loss of accuracy with respect to the approximation of the underlying sharp interface problem (1.4a–e). We illustrate this with an example for $\varepsilon^{-1} = 2\pi$ for the choice (2.11)(ii) together with $N_f = 256$, $N_c = 64$, $\tau = 10^{-2}$ and $T = 6$. The results are shown in Figure 6, where we observe a qualitative difference to the three previous simulations.

For the remainder of the simulations in this subsection we continue to employ (2.11)(ii), but we now choose $\rho = 0.01$. A simulation corresponding to Figure 6 can be seen in Figure 7. We observe that in this example, the presence of kinetic undercooling ($\rho > 0$)

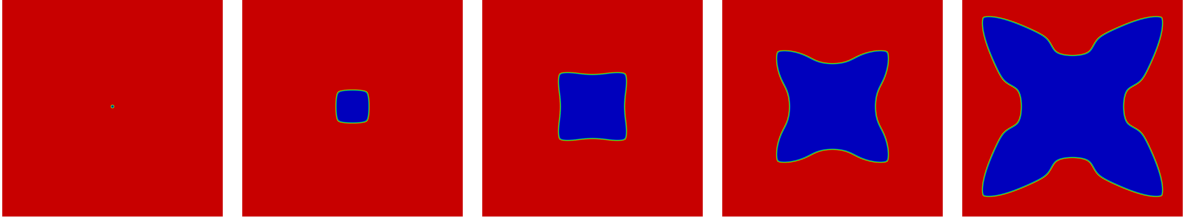


Figure 4: $(\varepsilon^{-1} = 8\pi, \text{ANI}_1^{(0.3)}, (2.11)(\text{ii}), \alpha = 0.03, \rho = 0, u_D = -2, \Omega = (-8, 8)^2)$
 Snapshots of the solution at times $t = 0, 1, 3, 5, 7$. [This computation took 4.5 hours.]

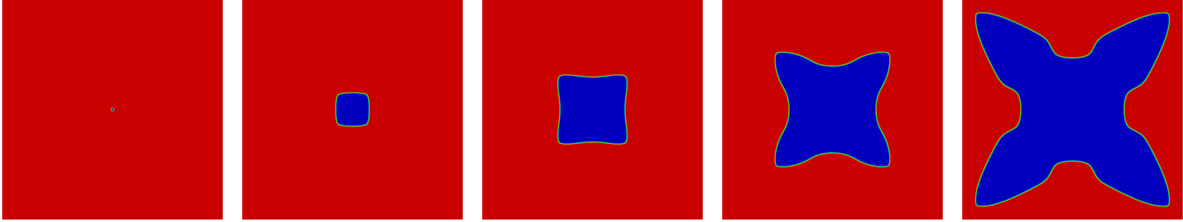


Figure 5: $(\varepsilon^{-1} = 8\pi, \text{ANI}_1^{(0.3)}, (2.11)(\text{iii}), \alpha = 0.03, \rho = 0, u_D = -2, \Omega = (-8, 8)^2)$
 Snapshots of the solution at times $t = 0, 1, 3, 5, 7$. [This computation took 10.5 hours.]

only has a small influence on the overall evolution.

The remaining computations in this subsection are for the rotated hexagonal anisotropy ANI_3^* . The first simulation is analogous to Figure 7, but now on the larger domain $\Omega = (-16, 16)^2$. In particular, we keep all the parameters as before, apart from γ and apart from $N_f = 512, N_c = 128$ due to the increased value of H . The results are shown in Figure 8. We have seen in previous simulations that the value of ε can have a large influence on the evolution of the phase field approximation. Reassuringly, in this example the evolution remains qualitatively unchanged if we repeat the simulation for $\varepsilon^{-1} = 4\pi$. A run with $N_f = 1024, N_c = 256, \tau = 10^{-3}$ and $T = 8$ is shown in Figure 9. We end this subsection with a repeat of the last computation, but now for the stronger supercooling $u_D = -4$. The evolution now exhibits six distinct side arms, as can be seen in Figure 10.

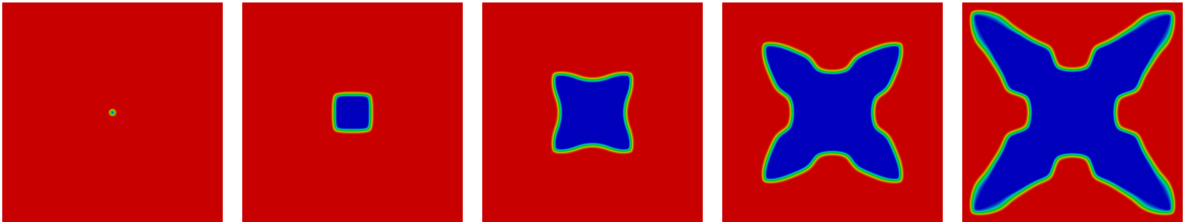


Figure 6: $(\varepsilon^{-1} = 2\pi, \text{ANI}_1^{(0.3)}, (2.11)(\text{ii}), \alpha = 0.03, \rho = 0, u_D = -2, \Omega = (-8, 8)^2)$
 Snapshots of the solution at times $t = 0, 1, 3, 5, 6$. [This computation took 3 minutes.]

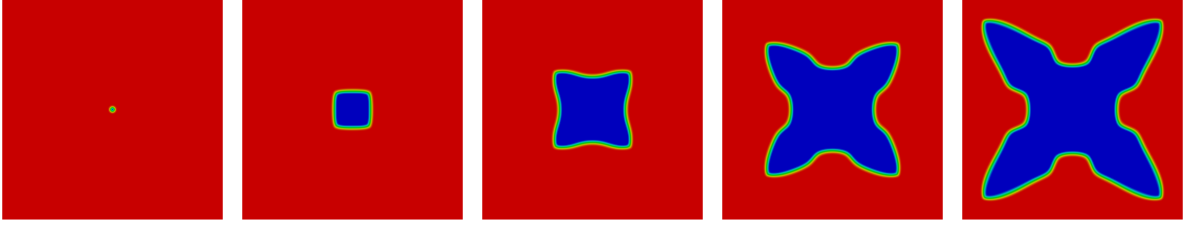


Figure 7: $(\varepsilon^{-1} = 2\pi, \text{ANI}_1^{(0.3)}, (2.11)(\text{ii}), \alpha = 0.03, \rho = 0.01, u_D = -2, \Omega = (-8, 8)^2)$
 Snapshots of the solution at times $t = 0, 1, 3, 5, 6$. [This computation took 4 minutes.]

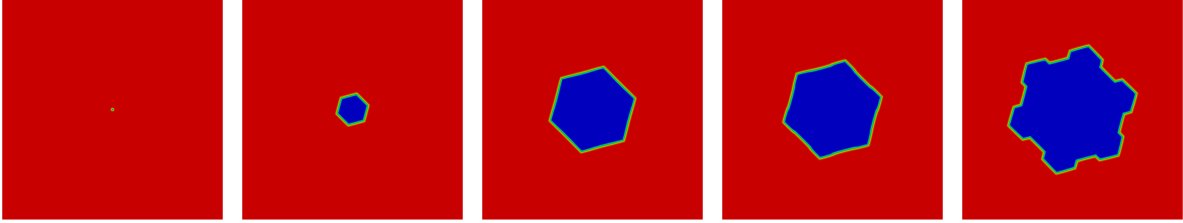


Figure 8: $(\varepsilon^{-1} = 2\pi, \text{ANI}_3^*, (2.11)(\text{ii}), \alpha = 0.03, \rho = 0.01, u_D = -2, \Omega = (-16, 16)^2)$
 Snapshots of the solution at times $t = 0, 1, 5, 6, 8$. [This computation took 25 minutes.]

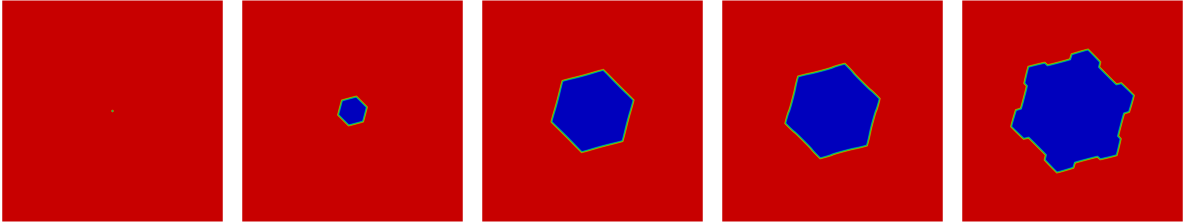


Figure 9: $(\varepsilon^{-1} = 4\pi, \text{ANI}_3^*, (2.11)(\text{ii}), \alpha = 0.03, \rho = 0.01, u_D = -2, \Omega = (-16, 16)^2)$
 Snapshots of the solution at times $t = 0, 1, 5, 6, 8$. [This computation took 5 hours, 17 minutes.]

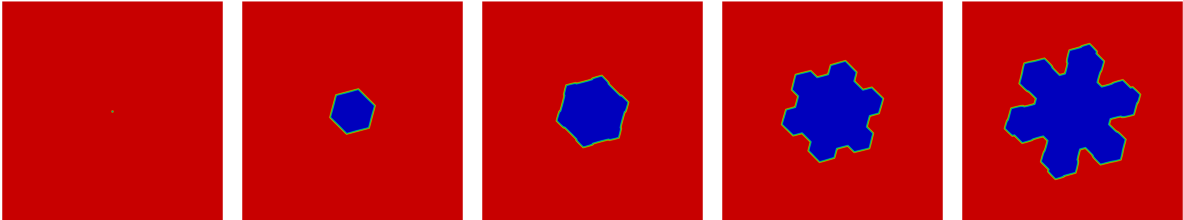


Figure 10: $(\varepsilon^{-1} = 4\pi, \text{ANI}_3^*, (2.11)(\text{ii}), \alpha = 0.03, \rho = 0.01, u_D = -4, \Omega = (-16, 16)^2)$
 Snapshots of the solution at times $t = 0, 1, 2, 3, 4$. [This computation took 3 hours, 5 minutes.]

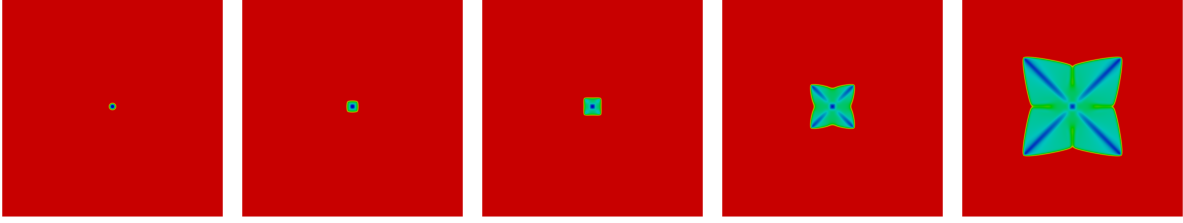


Figure 11: ($\varepsilon^{-1} = 4\pi$, $\text{ANI}_1^{(0.3)}$, (2.11)(ii), $\alpha = 5 \times 10^{-4}$, $\rho = 0.01$, $u_D = -0.5$, $\Omega = (-8, 8)^2$) Snapshots of the solution at times $t = 0, 0.1, 0.2, 0.5, 1$. [This computation took 76 minutes.]

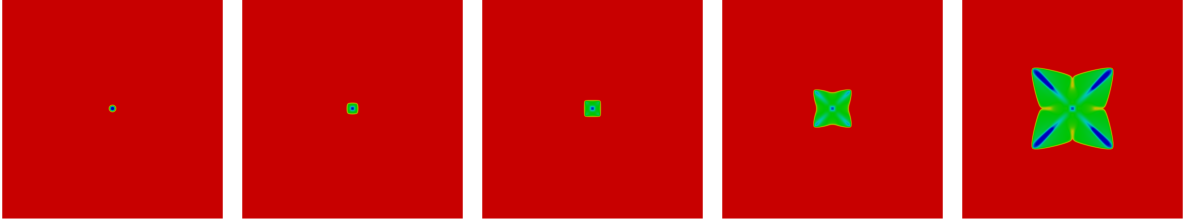


Figure 12: ($\varepsilon^{-1} = 4\pi$, $\text{ANI}_1^{(0.3)}$, (2.11)(iii), $\alpha = 5 \times 10^{-4}$, $\rho = 0.01$, $u_D = -0.5$, $\Omega = (-8, 8)^2$) Snapshots of the solution at times $t = 0, 0.1, 0.2, 0.5, 1$. [This computation took 165 minutes.]

5.2 Stefan problem in two space dimensions

In a first simulation for the full Stefan problem, i.e. with $\vartheta > 0$, we take parameters that are close to the ones used in Barrett *et al.* (2010b, Fig. 10). In particular, we have $\vartheta = 1$, $\alpha = 5 \times 10^{-4}$, $\rho = 0.01$, $u_D = -0.5$ and $R_0 = 0.2$, $H = 8$. An experiment with $\varepsilon^{-1} = 4\pi$ together with $N_f = 512$, $N_c = 64$, $\tau = 10^{-3}$ and $T = 1$ is shown in Figure 11, where we employ (2.11)(ii). We observe a very large interfacial region, which indicates that ε was not chosen small enough. A similar behaviour can be observed for the choice (2.11)(iii), see Figure 12. Here we note that in this example, in line with the analysis in (2.16), there appears to be no benefit in using (2.11)(iii) over (2.11)(ii). On reducing the size of the interfacial parameter ε , the phase field again assumes its expected profile across the interface, and we obtain the following numerical results. If $\varepsilon^{-1} = 16\pi$ together with $N_f = 2048$, $N_c = 128$, $\tau = 10^{-4}$ and $T = 2$ we obtain the results shown in Figure 13. If $\varepsilon^{-1} = 32\pi$ together with $N_f = 4096$, $N_c = 128$, $\tau = 10^{-4}$ and $T = 2$ we obtain the results shown in Figure 14. We can see that the small oscillations present in the final snapshot in Figure 13 have vanished in the corresponding plot in Figure 14. A closer comparison of the two solutions at time $t = 2$ can be seen in Figure 15.

The next simulation is for the rotated hexagonal anisotropy ANI_3^* . All the remaining parameters are as in Figure 13, i.e. $\varepsilon^{-1} = 16\pi$ together with $N_f = 2048$, $N_c = 128$, $\tau = 10^{-4}$ and $T = 2$. See Figure 16 for the numerical results. The large mushy regions in the final plot in Figure 16 indicate once again that ε needs to be chosen smaller. Hence we repeat this experiment and now choose $\varepsilon^{-1} = 32\pi$ together with $N_f = 4096$,

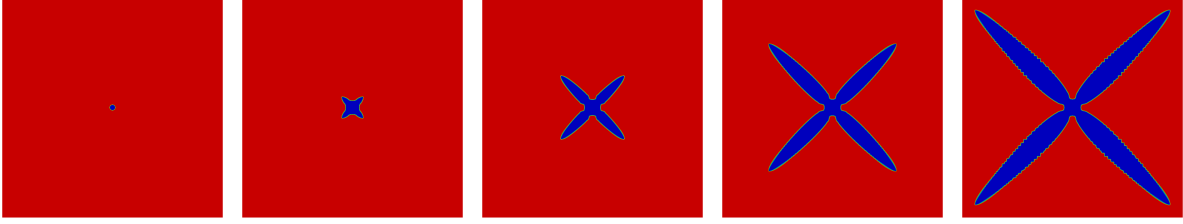


Figure 13: $(\varepsilon^{-1} = 16\pi, \text{ANI}_1^{(0.3)}, (2.11)(\text{ii}), \alpha = 5 \times 10^{-4}, \rho = 0.01, u_D = -0.5, \Omega = (-8, 8)^2)$ Snapshots of the solution at times $t = 0, 0.5, 1, 1.5, 2$. [This computation took 15.5 hours.]

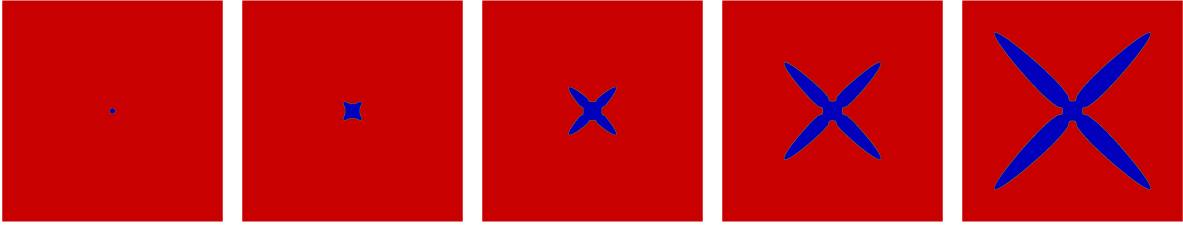


Figure 14: $(\varepsilon^{-1} = 32\pi, \text{ANI}_1^{(0.3)}, (2.11)(\text{ii}), \alpha = 5 \times 10^{-4}, \rho = 0.01, u_D = -0.5, \Omega = (-8, 8)^2)$ Snapshots of the solution at times $t = 0, 0.5, 1, 1.5, 2$. [This computation took 19.5 hours.]

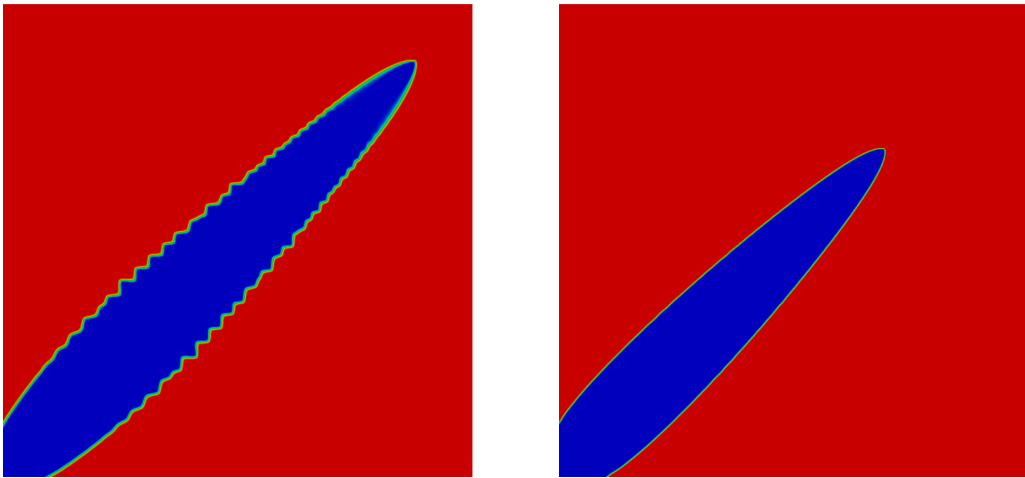


Figure 15: A close comparison of the final solutions from Figures 13 and 14. On the left $\varepsilon^{-1} = 16\pi$, and on the right $\varepsilon^{-1} = 32\pi$.

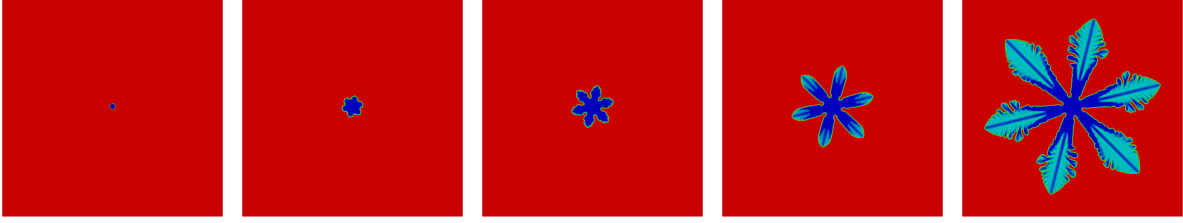


Figure 16: ($\varepsilon^{-1} = 16\pi$, ANI_3^* , (2.11)(ii), $\alpha = 5 \times 10^{-4}$, $\rho = 0.01$, $u_D = -0.5$, $\Omega = (-8, 8)^2$) Snapshots of the solution at times $t = 0, 0.5, 1, 1.5, 2$. [This computation took 51 hours.]

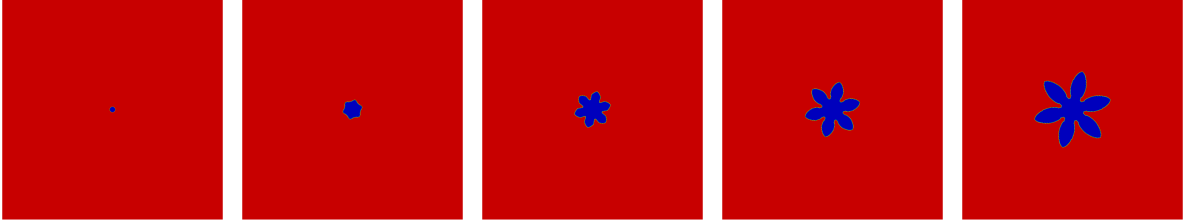


Figure 17: ($\varepsilon^{-1} = 32\pi$, ANI_3^* , (2.11)(ii), $\alpha = 5 \times 10^{-4}$, $\rho = 0.01$, $u_D = -0.5$, $\Omega = (-8, 8)^2$) Snapshots of the solution at times $t = 0, 0.5, 1, 1.5, 2$. [This computation took 19 hours.]

$N_c = 128$, $\tau = 10^{-4}$ and $T = 2$. See Figure 17 for the numerical results. We observe that the interfacial region is now well defined and that the evolution exhibits six distinct side arms.

5.3 Mullins–Sekerka in three space dimensions

In this subsection we always employ (2.11)(ii), and we always let $\vartheta = 0$. At first we also choose $\rho = 0$, so that we approximate a Mullins–Sekerka problem without kinetic undercooling. A simulation for the cubic anisotropy ANI_9 with $\varepsilon^{-1} = 2\pi$, and for the physical parameters $\alpha = 0.03$ and $u_D = -2$, can be seen in Figure 18. The discretization parameters are $N_f = 256$, $N_c = 64$, $\tau = 10^{-3}$ and $T = 1$. We observe that the cubic anisotropy induces the growth of the typical six symmetric side arms. If we repeat the simulation with $\rho = 0.01$, which models the presence of kinetic undercooling, the shape of the phase field approximation of the growing crystal changes significantly. We present a run for the discretization parameters $N_f = 256$, $N_c = 64$, $\tau = 10^{-2}$ and $T = 2$ in Figure 19. Note that the larger time step size used here yields a large reduction in the overall CPU time.

A repeat of the simulation in Figure 19, but now for the rotated hexagonal anisotropy ANI_4^* can be seen in Figure 20. In this simulation we can observe facet breaking, both in the basal and in the prismatic directions, similarly to the sharp interface computation shown in Barrett *et al.* (2012b, Fig. 18). With the next simulation we wish to highlight the effect that the choice of the mobility coefficient β can have on the evolution. If we

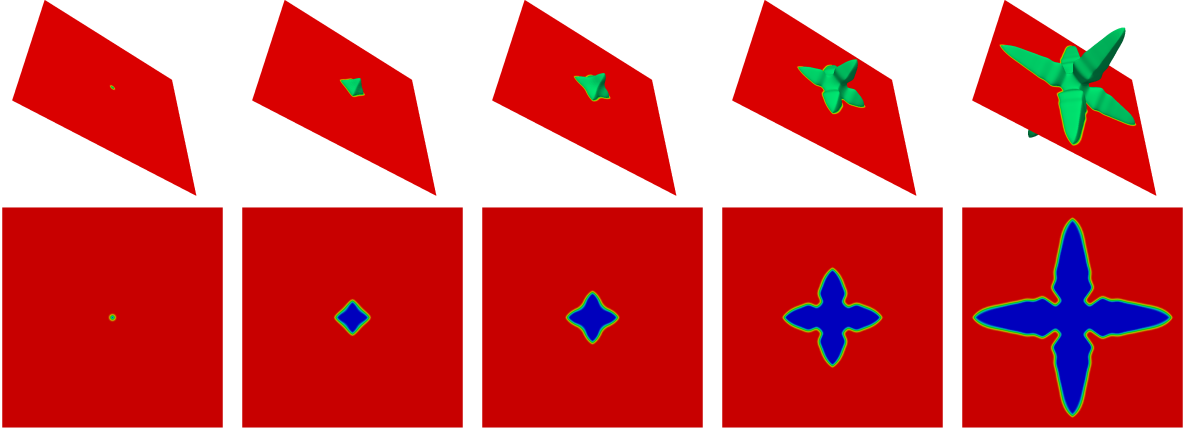


Figure 18: ($\varepsilon^{-1} = 2\pi$, ANI₉, (2.11)(ii), $\alpha = 0.03$, $\rho = 0$, $u_D = -2$, $\Omega = (-8, 8)^3$) Snapshots of the solution at times $t = 0, 0.1, 0.2, 0.5, 1$. [This computation took 13 days.]

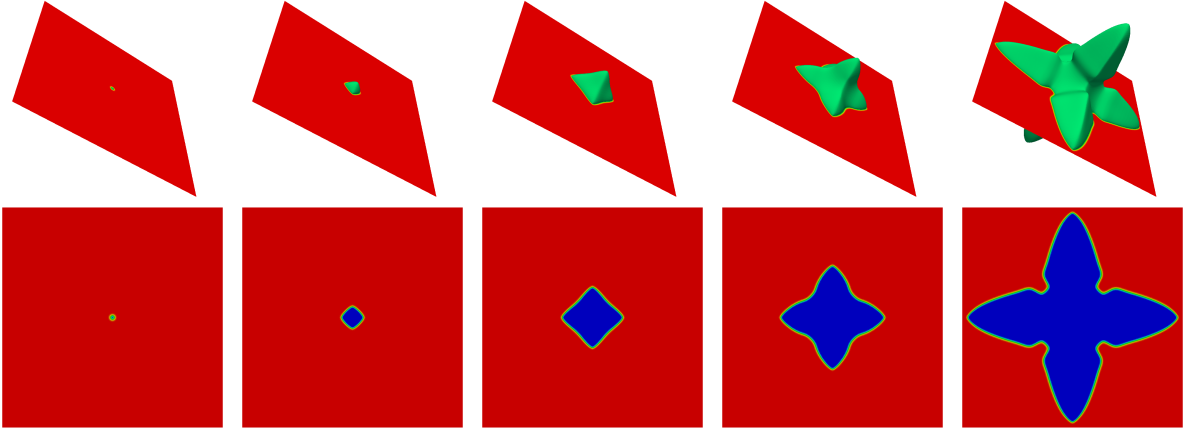


Figure 19: ($\varepsilon^{-1} = 2\pi$, ANI₉, (2.11)(ii), $\alpha = 0.03$, $\rho = 0.01$, $u_D = -2$, $\Omega = (-8, 8)^3$) Snapshots of the solution at times $t = 0, 0.1, 0.5, 1, 2$. [This computation took 4 days.]

replace $\beta = \gamma$ with $\beta = \beta_{\text{flat},3}$, where

$$\beta_{\text{flat},\ell}(p) := [p_1^2 + p_2^2 + 10^{-2\ell} p_3^2]^{\frac{1}{2}} \quad \forall p \in \mathbb{R}^d$$

is defined as in Barrett *et al.* (2012b, Eq. (16)), and if we keep all of the remaining parameters as before, then we obtain the results shown in Figure 21. Clearly, the growing crystal now assumes the shape of a flat prism. Similarly, if we choose the mobility coefficient $\beta = \beta_{\text{tall},2}$, where

$$\beta_{\text{tall},\ell}(p) := [10^{-2\ell} (p_1^2 + p_2^2) + p_3^2]^{\frac{1}{2}} \quad \forall p \in \mathbb{R}^d$$

is defined as in Barrett *et al.* (2012b, Eq. (17)), then we obtain the simulation presented in Figure 22. This time the initially spherical crystal grows into a tall hexagonal prism. It is discussed in Libbrecht (2005) that different mobility coefficients β are responsible for

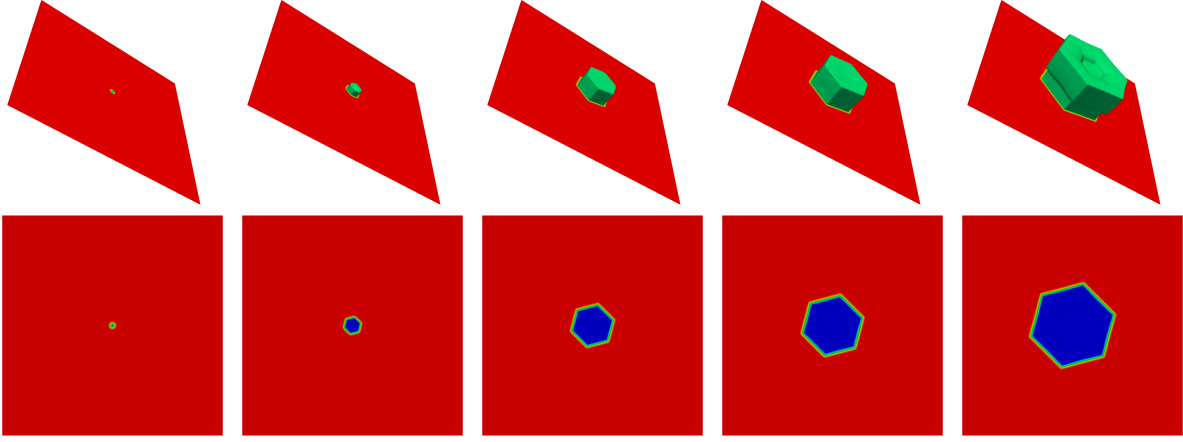


Figure 20: ($\varepsilon^{-1} = 2\pi$, ANI_4^* , (2.11)(ii), $\alpha = 0.03$, $\rho = 0.01$, $u_D = -2$, $\Omega = (-8, 8)^3$) Snapshots of the solution at times $t = 0, 0.1, 0.5, 1, 2$. [This computation took 22 hours.]

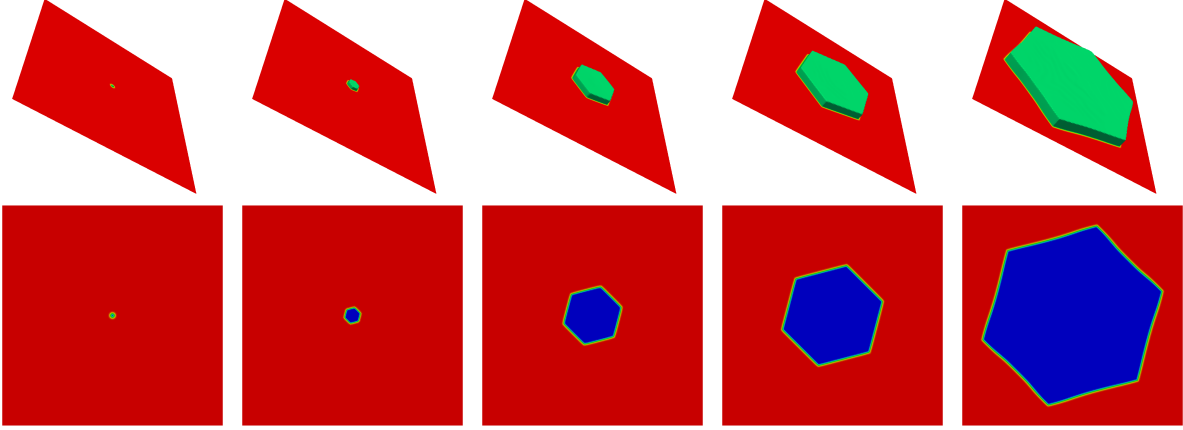


Figure 21: ($\varepsilon^{-1} = 2\pi$, ANI_4^* , (2.11)(ii), $\alpha = 0.03$, $\rho = 0.01$, $u_D = -2$, $\Omega = (-8, 8)^3$) Snapshots of the solution at times $t = 0, 0.1, 0.5, 1, 2$. [This computation took 2 days.]

the various snow crystal shapes seen in nature. In this context we remark that (1.4a–e) also appears in solidification from a supersaturated solution. In this case $-u$ is a suitably scaled concentration with $-u_D$ being the scaled supersaturation, see e.g. Barrett *et al.* (2012b) for more details.

5.4 Stefan problem in three space dimensions

In this subsection we present a simulation for the full Stefan problem in three space dimensions for the anisotropy ANI_9 . To this end, we consider the physical parameters $\vartheta = 1$, $\alpha = 10^{-3}$, $\rho = 0.01$, $u_D = -0.5$ and let $\Omega = (-4, 4)^3$. A numerical computation for $\varepsilon^{-1} = 16\pi$, together with $N_f = 1024$, $N_c = 64$, $\tau = 10^{-4}$ and $T = 0.4$ can be seen in Figure 23. Similarly to the results in Figure 19 we observe that the growing crystal

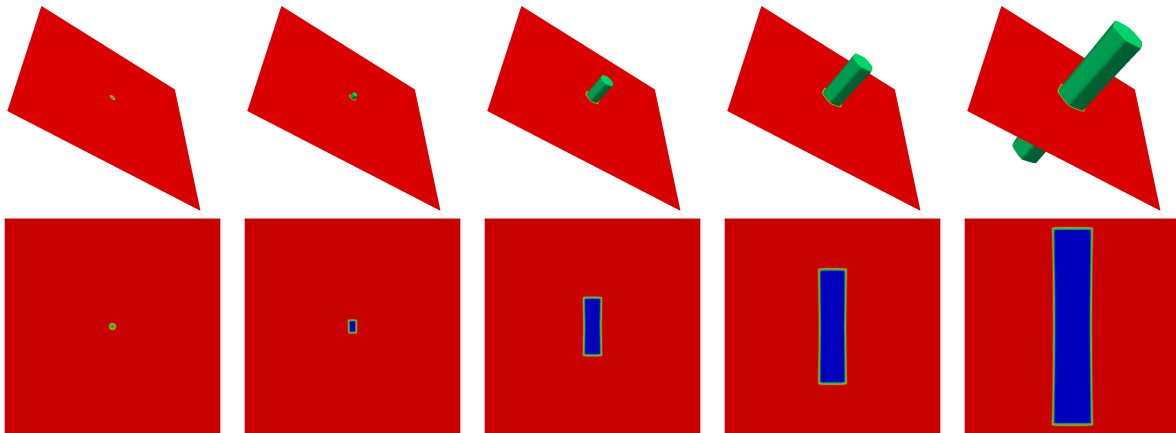


Figure 22: ($\varepsilon^{-1} = 2\pi$, ANI_4^* , (2.11)(ii), $\alpha = 0.03$, $\rho = 0.01$, $u_D = -2$, $\Omega = (-8, 8)^3$) Snapshots of the solution at times $t = 0, 0.1, 0.5, 1, 1.8$. [This computation took 26 hours.]

exhibits the typical six symmetric side arms that are common in simulations of dendritic growth.

References

- Amestoy, P. R., Davis, T. A., and Duff, I. S. (2004). Algorithm 837: AMD, an approximate minimum degree ordering algorithm. *ACM Trans. Math. Software*, **30**(3), 381–388.
- Bañas, L. and Nürnberg, R. (2008). Finite element approximation of a three dimensional phase field model for void electromigration. *J. Sci. Comp.*, **37**(2), 202–232.
- Bañas, L. and Nürnberg, R. (2009a). A multigrid method for the Cahn–Hilliard equation with obstacle potential. *Appl. Math. Comput.*, **213**(2), 290–303.
- Bañas, L. and Nürnberg, R. (2009b). Phase field computations for surface diffusion and void electromigration in \mathbb{R}^3 . *Comput. Vis. Sci.*, **12**(7), 319–327.
- Barrett, J. W., Blowey, J. F., and Garcke, H. (1999). Finite element approximation of the Cahn–Hilliard equation with degenerate mobility. *SIAM J. Numer. Anal.*, **37**(1), 286–318.
- Barrett, J. W., Nürnberg, R., and Styles, V. (2004). Finite element approximation of a phase field model for void electromigration. *SIAM J. Numer. Anal.*, **42**(2), 738–772.
- Barrett, J. W., Garcke, H., and Nürnberg, R. (2008a). Numerical approximation of anisotropic geometric evolution equations in the plane. *IMA J. Numer. Anal.*, **28**(2), 292–330.

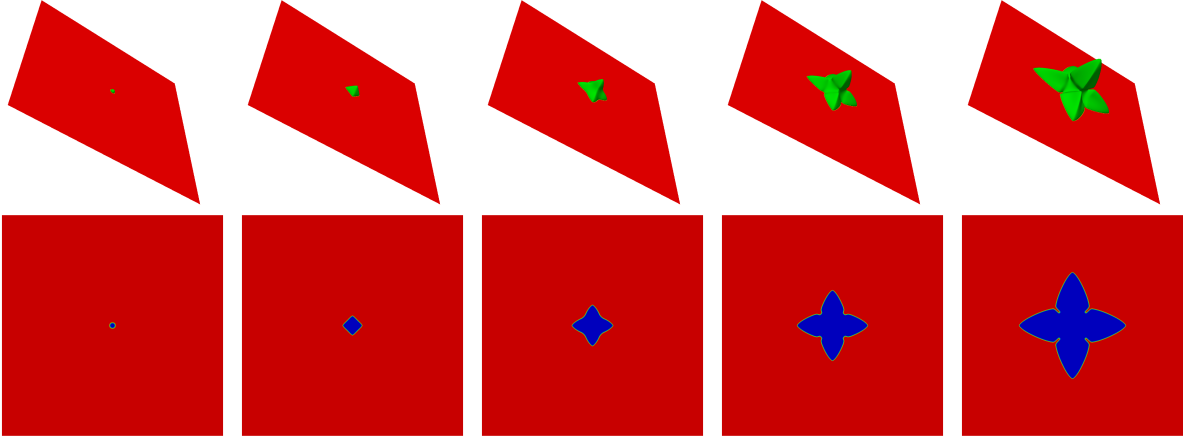


Figure 23: ($\varepsilon^{-1} = 16\pi$, ANI_9 , (2.11)(ii), $\alpha = 10^{-3}$, $\rho = 0.01$, $u_D = -0.5$, $\Omega = (-4, 4)^3$) Snapshots of the solution at times $t = 0, 0.1, 0.2, 0.3, 0.4$. [This computation took 20 days.]

Barrett, J. W., Garcke, H., and Nürnberg, R. (2008b). A variational formulation of anisotropic geometric evolution equations in higher dimensions. *Numer. Math.*, **109**(1), 1–44.

Barrett, J. W., Garcke, H., and Nürnberg, R. (2010a). Finite element approximation of coupled surface and grain boundary motion with applications to thermal grooving and sintering. *European J. Appl. Math.*, **21**(6), 519–556.

Barrett, J. W., Garcke, H., and Nürnberg, R. (2010b). On stable parametric finite element methods for the Stefan problem and the Mullins–Sekerka problem with applications to dendritic growth. *J. Comput. Phys.*, **229**(18), 6270–6299.

Barrett, J. W., Garcke, H., and Nürnberg, R. (2010c). Parametric approximation of surface clusters driven by isotropic and anisotropic surface energies. *Interfaces Free Bound.*, **12**(2), 187–234.

Barrett, J. W., Garcke, H., and Nürnberg, R. (2012a). Finite element approximation of one-sided Stefan problems with anisotropic, approximately crystalline, Gibbs–Thomson law. *Adv. Differential Equations*. (to appear), see also <http://arxiv.org/abs/1201.1802>.

Barrett, J. W., Garcke, H., and Nürnberg, R. (2012b). Numerical computations of faceted pattern formation in snow crystal growth. *Phys. Rev. E*, **86**(1), 011604.

Barrett, J. W., Garcke, H., and Nürnberg, R. (2012c). On the stable discretization of strongly anisotropic phase field models with applications to crystal growth. <http://arxiv.org/abs/1208.1147>.

Bellettini, G. and Paolini, M. (1996). Anisotropic motion by mean curvature in the context of Finsler geometry. *Hokkaido Math. J.*, **25**(3), 537–566.

- Blank, L., Butz, M., and Garcke, H. (2011). Solving the Cahn–Hilliard variational inequality with a semi-smooth Newton method. *ESAIM Control Optim. Calc. Var.*, **17**(4), 931–954.
- Blowey, J. F. and Elliott, C. M. (1992). The Cahn–Hilliard gradient theory for phase separation with non-smooth free energy. Part II: Numerical analysis. *European J. Appl. Math.*, **3**(2), 147–179.
- Boettinger, W. J., Warren, J. A., Beckermann, C., and Karma, A. (2002). Phase-field simulation of solidification. *Annu. Rev. Mater. Res.*, **32**, 163–194.
- Caginalp, G., Chen, X., and Eck, C. (2008). Numerical tests of a phase field model with second order accuracy. *SIAM J. Appl. Math.*, **68**(6), 1518–1534.
- Cahn, J. W. and Hoffman, D. W. (1974). A vector thermodynamics for anisotropic surfaces – II. Curved and faceted surfaces. *Acta Metall.*, **22**(10), 1205–1214.
- Chen, L.-Q. (2002). Phase-field models for microstructure evolution. *Annu. Rev. Mater. Res.*, **32**, 113–140.
- Davis, T. A. (2004). Algorithm 832: UMFPACK V4.3—an unsymmetric-pattern multi-frontal method. *ACM Trans. Math. Software*, **30**(2), 196–199.
- Davis, T. A. (2005). Algorithm 849: a concise sparse Cholesky factorization package. *ACM Trans. Math. Software*, **31**(4), 587–591.
- Deckelnick, K., Dziuk, G., and Elliott, C. M. (2005). Computation of geometric partial differential equations and mean curvature flow. *Acta Numer.*, **14**, 139–232.
- Eck, C., Garcke, H., and Stinner, B. (2006). Multiscale problems in solidification processes. In *Analysis, modeling and simulation of multiscale problems*, pages 21–64. Springer, Berlin.
- Elliott, C. M. (1997). Approximation of curvature dependent interface motion. In I. S. Duff and G. A. Watson, editors, *The state of the art in numerical analysis (York, 1996)*, volume 63 of *Inst. Math. Appl. Conf. Ser. New Ser.*, pages 407–440. Oxford Univ. Press, New York.
- Elliott, C. M. and Gardiner, A. R. (1996). Double obstacle phase field computations of dendritic growth. University of Sussex CMAIA Research report 96-19, <http://homepages.warwick.ac.uk/staff/C.M.Elliott/PAPERS/DoubleObstaclePhaseField/El1Gar96.pdf>.
- Elliott, C. M. and Schätzle, R. (1996). The limit of the anisotropic double-obstacle Allen-Cahn equation. *Proc. Roy. Soc. Edinburgh Sect. A*, **126**(6), 1217–1234.
- Elliott, C. M. and Stuart, A. M. (1993). The global dynamics of discrete semilinear parabolic equations. *SIAM J. Numer. Anal.*, **30**(6), 1622–1663.

- Garcke, H. and Stinner, B. (2006). Second order phase field asymptotics for multi-component systems. *Interfaces Free Bound.*, **8**(2), 131–157.
- Gräser, C. and Kornhuber, R. (2007). On preconditioned Uzawa-type iterations for a saddle point problem with inequality constraints. In *Domain decomposition methods in science and engineering XVI*, volume 55 of *Lect. Notes Comput. Sci. Eng.*, pages 91–102. Springer, Berlin.
- Gräser, C., Kornhuber, R., and Sack, U. (2012). Nonsmooth Schur–Newton methods for vector-valued Cahn–Hilliard equations. Matheon Preprint, Berlin.
- Gurtin, M. E. (1988). Multiphase thermomechanics with interfacial structure. 1. Heat conduction and the capillary balance law. *Arch. Rational Mech. Anal.*, **104**(3), 195–221.
- Hintermüller, M., Hinze, M., and Tber, M. H. (2011). An adaptive finite-element Moreau–Yosida-based solver for a non-smooth Cahn–Hilliard problem. *Optim. Methods Softw.*, **26**(4-5), 777–811.
- Karma, A. and Rappel, W.-J. (1996). Phase-field method for computationally efficient modeling of solidification with arbitrary interface kinetics. *Phys. Rev. E*, **53**(4), R3017–R3020.
- Karma, A. and Rappel, W.-J. (1998). Quantitative phase-field modeling of dendritic growth in two and three dimensions. *Phys. Rev. E*, **57**(4), 4323–4349.
- Kim, J., Kang, K., and Lowengrub, J. (2004). Conservative multigrid methods for Cahn–Hilliard fluids. *J. Comput. Phys.*, **193**(2), 511–543.
- Kobayashi, R. (1993). Modeling and numerical simulations of dendritic crystal growth. *Phys. D*, **63**(3-4), 410–423.
- Kornhuber, R. (1994). Monotone multigrid methods for elliptic variational inequalities I. *Numer. Math.*, **69**, 167–184.
- Langer, J. S. (1986). Models of pattern formation in first-order phase transitions. In *Directions in condensed matter physics*, volume 1 of *World Sci. Ser. Dir. Condensed Matter Phys.*, pages 165–186. World Sci. Publishing, Singapore.
- Li, B., Lowengrub, J., Rätz, A., and Voigt, A. (2009). Geometric evolution laws for thin crystalline films: modeling and numerics. *Commun. Comput. Phys.*, **6**(3), 433–482.
- Libbrecht, K. G. (2005). The physics of snow crystals. *Rep. Progr. Phys.*, **68**(4), 855–895.
- Luckhaus, S. (1990). Solutions for the two-phase Stefan problem with the Gibbs–Thomson law for the melting temperature. *European J. Appl. Math.*, **1**(2), 101–111.
- McFadden, G. B. (2002). Phase-field models of solidification. In *Recent advances in numerical methods for partial differential equations and applications (Knoxville, TN, 2001)*, volume 306 of *Contemp. Math.*, pages 107–145. Amer. Math. Soc., Providence, RI.

- McFadden, G. B., Wheeler, A. A., Braun, R. J., Coriell, S. R., and Sekerka, R. F. (1993). Phase-field models for anisotropic interfaces. *Phys. Rev. E* (3), **48**(3), 2016–2024.
- Mullins, W. W. and Sekerka, R. F. (1963). Morphological stability of a particle growing by diffusion or heat flow. *J. Appl. Phys.*, **34**(2), 323–329.
- Penrose, O. and Fife, P. C. (1990). Thermodynamically consistent models of phase-field type for the kinetics of phase transitions. *Phys. D*, **43**(1), 44–62.
- Schmidt, A. and Siebert, K. G. (2005). *Design of Adaptive Finite Element Software: The Finite Element Toolbox ALBERTA*, volume 42 of *Lecture Notes in Computational Science and Engineering*. Springer-Verlag, Berlin.
- Singer-Loginova, I. and Singer, H. M. (2008). The phase field technique for modeling multiphase materials. *Rep. Progr. Phys.*, **71**, 106501 (32 pages).
- Torabi, S., Lowengrub, J., Voigt, A., and Wise, S. (2009). A new phase-field model for strongly anisotropic systems. *Proc. R. Soc. Lond. Ser. A Math. Phys. Eng. Sci.*, **465**(2105), 1337–1359.
- Wang, S.-L., Sekerka, R., Wheeler, A., Murray, B., Coriell, S., Braun, R., and McFadden, G. (1993). Thermodynamically-consistent phase-field models for solidification. *Phys. D*, **69**(1–2), 189–200.
- Wheeler, A. A. and McFadden, G. B. (1996). A ξ -vector formulation of anisotropic phase-field models: 3D asymptotics. *European J. Appl. Math.*, **7**(4), 367–381.